Ph.D. Dissertation of Engineering

DEVELOPTMENT OF HYDROGEL-SOLID HYBRIDS FOR ELECTRO-MICROFLUIDICS AND SINGLE CELL ANALYSIS

전기-미세유체 및 단일세포분석 시스템을 위한 하이드로젤-고체 하이브리드 개발

August 2020

INTERDISCIPLINARY PROGRAM FOR
BIOENGINEERING
GRADUATE SCHOOL
SEOUL NATIONAL UNIVERSITY
SANGWOOK BAE

Abstract

Agarose and other noncovalent hydrogels have good biocompatibility but their applications were restricted since they tend to have low interfacial bonding strength with other polymers or solids. Previously introduced noncovalent hydrogel-to-solid fixation strategies relied heavily on mechanical clamping which is a temporary approach and difficult to apply to kinetic parts or morphologically non-trivial adhesions. Here, we introduce a facile method that increased interfacial bonding strength of agarose hydrogel against solids via an interface-toughening hydrogel. The method showed applicability to several other noncovlanet hydrogels as well, including gelatin, alginate, agar, and chitosan. The bonding method requires no mechanical clamping, liquid glue or bulk modification of the noncovalent hydrogel's polymer backbone. It is also compatible with forming micropatterns within the bonding interface. With this new bonding technique, we were able to fabricate various noncovalent hydrogel-solid integrated structures with novel functionalities for in vitro assay, soft robotics and biologically inspired systems.

Keywords: Noncovalent Hydrogel, interpenetrating network, Electro-microfluidics

Student Number: 2014-31113

Contents

Chapter 1 ..... **1**

Chapter 2 ..... **6**

2.1 Fabrication of hybrid hydrogel films 7
2.2 Fabrication of hybrid hydrogel and noncovalent hydrogel double layer structure 8
2.3 Performing various hydrogel-to-hybrid gel bonding 8
2.4 Agarose hydrogel to tough hydrogel bonding procedure. 9
2.5 Preparing solids and elastomers to bond with hybrid gels. 10

Chapter 3 ..... **11**

3.1 FTIR measurement of imine bond formation 12
3.1.1 Sample preparation for FTIR measurement 12
3.1.2 FTIR Measurement result 12
3.2 13C-NMR chemical shift measurement 15
3.2.1 Sample preparation for NMR measurement 15
3.2.2 NMR measurement result 16
3.3 SEM/EDS measurement of monomer diffusion layer 19
3.3.1 Sample preparation for SEM measurement 19
3.3.2 SEM measurement result 19
3.3.3 EDS measurement result 21

Chapter 4 25

4.1 Bonding strength measurement 26
4.1.1 The effect of monomer concentration 26
4.1.2 The effect of agarose chain aldehyde modification 30
4.1.3 The effect of monomer diffusion 31
4.1.4 Fracture energy analysis 33
4.2 Noncovalent hydrogel to solid bonding 35
4.2.1 Noncovalent hydrogel to solid surface bonding 35
4.2.2 Noncovalent hydrogel to elastomer surface bonding 36
4.2.3 Noncovalent hydrogel to tough hydrogel bonding 41

Chapter 5 45

5.1 Zig-free hydrogel microfluidic system 46
5.2 Electrophoretic oligonucleotide retrieval system 52
5.3 Discussion 57

Chapter 6 59

6.1 Introduction of the field and the proposed approach 59
6.2 Device design 62
6.2.1 Optimization of cell assembly protocol 66
6.2.2 Optimization of electrophoretic mRNA capture protocol 70
6.2.3 Crosslinking mRNA capturing probe onto magnetic microparticles 74
6.2.4 Optimizing RT-PCR protocol for single cell or small number of cells using mouth pipetting 75
6.2.5 Critical limitation of the approach 80

Chapter 7 81

7.1 Single cell electrophoresis protocol optimization 82

7.1.1 Optimization of barcoded mRNA-capturing microparticle synthesis 82

7.1.2 Optimization of cell assembly and bead assembly 87

7.1.3 Optimization of electrophoretic mRNA capture protocol 93

7.2 Single cell RNA retrieval demonstration 96

7.2.1 Single cell mRNA retrieval test 96

7.2.2 Bead harvest and RT-PCR 105

7.2.3 Validation using Sanger sequencing 107

7.2.4 Discussion 110

Chapter 8 : Summary 115

Bibliography 117

Abstract(국문초록) 120

List of Figures

Figure 1. Schematic of noncovalent hydrogel to hybrid hydrogel bonding. 3

Figure 2. Description of agarose aldehyde activation and forming imine bond (Schiff base) with polyacrylamide chain 13

Figure 3. FT-IR measurement result. The C=N bond was specifically increased in the hybrid hydrogel sample. SP: sodium periodate. PAAm: Polyacrylamide. 4d: 4-day treatment..... 14

Figure 4. Agarose and aldehyde-agarose NMR measurement simulation and actual result. A shows the simulation result based on agarose chain structure. B,C each shows the actual NMR shift spectrum of normal agarose and aldehyde-activated agarose. The red box in C shows the aldehyde peak..... 17

Figure 5. Comparison of hybrid gel NMR peaks with peaks from agarose, aldehyde-agarose and PAAm. Yellow triangles indicate aldehyde-agarose specific peaks including the 209 ppm peak. Red arrow indicates the hybrid gel specific peak..... 18

Figure 6. SEM image of the agarose/hybrid gel intermediate. 20

Figure 7. . EDS image of the agarose/hybrid hydrogel interface. From left to right is the original SEM image, Sodium (N), Oxygen (O), Sulfur(S), Potassium (K) image. Each row are images from the same sample. 20

Figure 8. EDS line scanning data. The EDS scan was done on the SEM image (below) along the given arrow line. From hybrid (H) to agarose (A), along the intermediate region, the Sulfur (S) and Potassium (K) concentration reduced gradually while O, N concentration didn't vary. 22

Figure 9. Fehling test based verification of aldehyde-agarose. Only the sodium periodate-treated agarose produced precipitant after reaction. 22

Figure 10. Jig design and sample preparation procedure. The jig is first bolted to the tensile tester using an M6 bolt. Then the hybrid gel or noncovalent hydrogel-bonded acryl plate is placed on the jig. Then a pair of fixing plates are bolted to the jig using M6 bolts. 27

Figure 11. Flatwise tensile test example schematic. The additional jig for the upside hydrogel is pre-assembled with an acryl plate that has been painted with fast glue and is carefully let to contact the upside hydrogel and let to fix for > 1 minutes. Then the actual tensile test is perforemed. 27

Figure 12. Bonding strength measurement with varying AAm monomer concentration within hybrid hydrogel. Sodium periodate treatment condition (3mM) was the same for all samples. 29

Figure 13. Bonding strength with varying sodium periodate concentration. 29

Figure 14. Raw extension-force curves for diffusion time variation (A), AAm concentration variation (B), and sodium periodate treatment

concentration variation (C). 32

Figure 15. AAm diffusion time variation bonding strength effect test. Left shows images of the varying intermediate region thickness with different diffusion time. Right shows the bonding strength with varying diffusion time. 32

Figure 16. Schematic explanation of the reason why diffusion time did not affect bonding strength. The debonding plane was always the plane between the agarose and hybrid hydrogel original contact surfaces, regardless of the monomer diffusion layer thickness or monomer concentration. 34

Figure 17. Fracture energy measurement of hybrid hydrogel. Sodium periodate concentration did not affect fracture energy of the hybrid hydrogel. 34

Figure 18. Schematic of noncovalent hydrogel to solid surface bonding. 36

Figure 19. Bonding hybrid hydrogel with various noncovalent hydrogel. In A, from left to right is alginate, gelatin, and agar hydrogel bonded to hybrid hydrogel slab. B shows the high bonding strength of gelatin to hybrid hydrogel. C shows the fracture of agar gel after bending test yet remaining bonded. 40

Figure 20. Bonding tough hydrogel with hybrid hydrogel or noncovalent hydrogel. A and B shows bonding tough hydrogel bonded to hybrid hydrogel. C shows a dumbbell shaped tough hydrogel bonded to a slab of agarose hydrogel. For C, the bonded structure showed stretchability

of around 310% before debonding between agarose and tough hydrogel. 43

Figure 21. Bonding tough hydrogel with agarose hydrogel in the presence or absence of TPP treatment. TPP treatment was critical for successful bonding between tough hydrogel and agarose hydrogel..... 44

Figure 22. Diffusive agarose microfluidic system without mechanical jig fixation. A shows the diffusive flow of Rhodamine B solution in a micropatterned agarose hydrogel system. B shows the diffusive flow of Rhodamine B solution in a micropatterned hybrid hydrogel system. C shows the bright field image of the channel after experiment. Control channel was a closed channel with no Rhodamine B flow. 47

Figure 23. Rhodamine B fluorescence intensity measured over time at the cross-section of the diffusive microfluidic agarose hydrogel system. 49

Figure 24. The microfluidic chip design for the diffusive agarose hydrogel system. A,B shows the bright field image. C shows target versus control channel flow experiment of FITC-conjugated streptavidin. 49

Figure 25. Design of the hollow cylinder-shaped raster-scanning microfluidic chip. The microchannel was patterned at the agarose hydrogel side..... 51

Figure 26. Experiment result of red dye solution flow into the raster

scanning microfluidic channel. 5 1

Figure 27. Schematic description of how hybrid pregel solution can be used for generating a tightly sealed noncovalent hydrogel inlet to glass tube connection..... 5 3

Figure 28. Design of the electrophoretic oligonucleotide retriever. The glass/plastic tubes for fluidic retrieval are inserted into the agarose/hybrid interface which is pre-patterned with a channel that goes through the path of oligonucleotide electrophoresis. As the sample is introduced into the sample inlet and electric field (red arrow) is introduced, the bands will move in the direction indicated in yellow arrow. And when the target band passes through the channel , fluidic flow can be introduced to retrieve the band. 5 3

Figure 29. Detailed step of electrophoretic oligonucleotide retrieval .. 5 4

Figure 30. Experiment result of electrophoretic double strand DNA (dsDNA) retrieval. From left to right, the gel image after 1.4kbp retrieval, the retrieved 1.4kbp dsDNA, retrieved 1kbp dsDNA, and 600bp dsDNA sample. 5 4

Figure 31. Schematic description of the verification experiment of double strand DNA dehybridization and mismatch rehybridization occurred during gel purification process. dsDNA with variant is dehybridized into ssDNA by chaotropic salt present in the gel melting solution and rehybridization by suspending in water leads to mismatch dsDNA (drawn as dsDNA with bulges). This mismatch can be broken into

shorter dsDNA by T7 endonuclease I. 56

Figure 32. Experiment result of T7 endonuclease I based mismatch dsDNA cleavage and yield comparison between conventional gel purification (Qiagen kit) and proposed fluidic retrieval. 56

Figure 33. . Initial design of sequential RNA, DNA retrieval from a single cell using agarose well and probe microparticle. The DNA could be either imaged with FISH or amplified by MDA and retrieved to another microparticle by electrophoresis 65

Figure 34. Mask design used for agarose micro well design. Either wells with diameter with 15um or 20um was designed. Using the mask I fabricated the negative pattern for microwell arrays (pillar arrays) using SU8 2015. From the pillar array, I poured on melted 1.5% agarose and let to solidify under ambient condition. The agarose well array was then peeled off and inspected under microscope..... 67

Figure 35. Fabrication process of agarose micro-well chip and example result. The SU8 pattern was molded into a PDMS mold. And the PDMS mold was then molded a second time with agarose hydrogel. The below four images are example of agarose wells..... 67

Figure 36. Example images of cell dispensed agarose array. The cells tended to assemble into the wells compared to non-well surfaces... 6

8

Figure 37. Example result of cell assembly before and after washing. The cells could be also stained with DNA or RNA staining materials such

as Hoecsht, SYTORNAstain, and Pyronin Y. The results are shown below where around 80-90% of wells are assembled with single cells 68

Figure 38. Example result of cell assembly with fluorescently stained cells. 69

Figure 39. Example Confocal image of Hoecsht and Pyronin Y stained cells. 72

Figure 40. Electrophoretic RNA selective retrieval demonstration using Hoechst/Pyronin Y stained cells. 72

Figure 41. Schematic example of cell array and bead array assembly. 73

Figure 42. Schematic example of electrophoresis from the assembled cell/bead array. 73

Figure 43. Example result of micropipette based cell retrieval and ejection..... 78

Figure 44. RT-PCR result from small number of cells. 10 cell sample was the RT-PCR result from 10 mouth-pipette retrieved cells. Pure RNA sample was the RT-PCR result from 300pg of purified RNA. NTC: no template control. PCR- : same condition with pure RNA sample but with no PCR. 78

Figure 45. RT-PCR result from on-bead mRNA capture and RT-PCR. 8

0

Figure 46. Procedure of synthesizing RNA capturing and barcoding magnetic microparticle (MMP) and RT-PCR of captured mRNA. The MMP contains carboxyl groups on the surface on which reverse amidite synthesis can initiate. The PCR primer (TSO) is synthesized first. Then cell barcodes are synthesized by a series of split pooling (usually 12 cycles). Then 10 cycles of random nucleotide synthesis creates unique molecular identifier (UMI) and 30 thymine is synthesized (step 1-4). After ammonium hydroxide based deprotection, the beads are ready for mRNA capturing. mRNA is captured by its poly A tail, then reverse transcriptase synthesizes cDNA and a triple C overhang. The template switch oligo (TSOrGrG+G) hybridizes to this overhang and template switching occurs. The TSO on both side is now used for PCR. 86

Figure 47. Method of preparing agarose-filled, bead assembled, microcapillary array. The glass microcapillary is first submerged in 1% TMSPMA solution for TMSPMA coating. Then the capillary is submerged in 1.5% low melting agarose (LMA) solution at 37°C overnight for filling the capillaries. Then the chip is removed from the solution and gelation occurs at room temperature. In the capillary wells, the beads are assembled by cell scraping while a strong magnet is placed on the opposite side. 89

Figure 48. Example image of bead assembled. The 18.9um diameter MMPs were assembled into the 20um diameter capillary wells with 70-90% filling rate. 90

Figure 49. Trials of two cell assembly methods. Simple dispensing (upper

row) ended up with most of the cells not aligning with the capillary wells. Cell scraping after cell dispensing (low row) ended up with damaged cells due to the high viscosity of agarose compared to water. 90

Figure 50. Third method of cell assembly using capillary flow based cell suction. Since the capillaries are open on both side, the cell medium (in this case DPBS) can penetrate into the capillary wells and exit through the bottom side of the capillaries. The exited medium can be soaked by paper tissues by capillary flow. This capillary flow induces the cell assembling effect. After the cells are assembled and the cell medium is mostly removed, a 1% LMA solution is dispensed and let for gelation which leads to cell sealing and physical fixation..... 91

Figure 51. Experiment result of third cell assembly method using capillary suction..... 92

Figure 52. A custom acrylic MCA holder. The four acrylic blockers are assembled. for creating the agarose blockers. The agarose filling chambers are filled with approximately 5% agarose solution and let for gelation. The blockers are removed and the MCA assembled with both cell and MMPs are assembled..... 95

Figure 53. Procedure of single cell mRNA capture and fluorescent tagging for imaging. First a lysis & hybridization solution containing detergent (usually 0.1-0.5% SDS), high salt (usually 100-500mM LiCl) and buffer (10x TE) is filled in the MCA chamber. Then an electric field (usually 1V/cm) is immediately turned on to transfer mRNA along the capillaries. After 10-20 minutes the mRNA hybridize onto the oligo probes on the MMPs. Then Cy30-T20 is introduced into the

MCA chamber for hybridization onto the poly A tails of the captured mRNA molecules. Therefore, the MMPs that contain the mRNA will be fluorescent. 98

Figure 54. Experiment result of mRNA capturing from single cells and fluorescent imaging. From both experiments (A-C and D), the fluorescence signals show digital patterns rather than continuous pattern. This indicates proper mRNA capture without cross contamination with adjacent capillaries. 101

Figure 55. Fluorescence intensity and standard curve based mRNA capture rate deduction of Single cell electrophoresis (SCE) experiment result. First the mRNA capturing probe concentration on these MMPs were measured with Qubit ssDNA kit. Then the fluorescence intensity of the MMPs of a positive control (saturating cy3T20 probe hybridization) and SCE result MMPs were measured with a fluorescence microscope and quantified with Image J. Then a standard curve was created using a serial dilution of Cy3 solution. The positive control (+CTRL) and SCE fluorescence was positioned at the standard curve to deduce the Cy3 probe concentration on the SCE MMPs. Then the number of Cy3 T20 probes hybridized onto a single mRNA molecule was used to finally deduce the number of mRNA molecules hybridized onto the MMPs. 104

Figure 56. Result of MMP retrieval method using sonication. 106

Figure 57. Method of retrieving the MMPs using a high concentration agarose film and peel-off. The resulting films can be directly used for reverse transcription and PCR since agarose does not prevent these reactions. 106

Figure 58. Sanger sequencing result of captured mRNA. 109

Figure 59. Circuitry of the electrophoresis device. 110

Figure 60. The model kit protocol part 1. The bead assembled MCA can be prepared by the kit manufacturer and distributed to users. Cells are assembled by simple dispensing by the user. 112

Figure 61. The model kit protocol part 2. The MCA is inserted into the electrophoresis device and the batteries are assembled as well.... 11

2

Figure 62. The top view after the MCA and batteries are assembled. The voltage regulator and timer is connected to the electrodes which are placed on both side of the MCA cell, bead array surfaces. 113

Figure 63. The model kit protocol part 3. The chamber is filled with buffer and electrophoresis is performed to capture the cell mRNA onto the RNA capturing beads. 113

Figure 64. Comparison of the commercialized kit and proposed method. Unlike the commercialized kit, proposed method doesn't require any live cell delivery and RNA capture QC can be done with lower price. 114

List of Tables

Table 1. Predicted impacts of high-throughput single cell analysis. Referred from Ehud Shapiro et al., Nat. Rev. Gen., 2013. 63

Table 2. Advantages of proposed single cell DNA/RNA retrieval method. 65

Table 1. Predicted impacts of high-throughput single cell analysis. Referred from Ehud Shapiro et al., Nat. Rev. Gen., 2013..... 63

Table 2. Advantages of proposed single cell DNA/RNA retrieval method. 65

Chapter 1

Introduction

Hydrogel materials are now being adapted to fields including soft robotics, and tissue engineering. As a sub-category, naturally derived `noncovalent hydrogels` have good biocompatibility and self-healing property. They are physically crosslinked hydrogels formed by weak bonds such as hydrogen bonds or ionic bonds. In case of agarose, although it tends to have poor mechanical properties, many biomimetic, fluidic systems integrated with these hydrogels were introduced due to their excellent biocompatibility. For example, microchannel patterned, or cell-laden agar/agarose gels were used in microsystems for cell culturing, organism imaging, point-of-care devices, or ordered assembly. Yet, applications of such purely noncovalent hydrogel was restricted since it tends to have low interfacial bonding strength with other polymers or solids. To overcome this problem, it becomes important to develope methods that would enable strong adhesion between agarose hydrogel and solid. Previously introduced hydrogel-to-solid fixation strategies could be categoriezed into either mechanical clamping or chemical adhesion. Mechanical clamping uses jigs to maintain contact between hydrogel and other solids without

slippage or bursting. But they are temporary approaches and for non-trival hydrogel-solid adhesions such as forming kinetic joints or sealing channel-tube junctions, it would be more effective to use chemical adhesion. Chemical adhesion approaches use external glues and/or incorporate solid-adhering functional groups into the hydrogel's polymer backbone. These recent advances in chemical hydrogel-solid adhesion techniques opened new opportunities for applying many hydrogels into microsystem designing. Concordantly, to develope new systems robustly integrated with noncovalent hydrogels, such as agarose, it would be desirable to develope a new chemical adhesion method that enables strong adhesion between solids and noncovalent hydrogels while preserving the bulk property of the hydrogel.

In this work, I introduce a facile method for increasing interfacial bonding strength of agarose hydrogel against solids via an interface-toughening hydrogel, designated as `hybrid hydrogel` (**Figure 1**). In other words, this hybrid hydrogel acts as a two-sided tape between agarose hydrogel and solids. Although we concentrated our analysis mostly on utilizing agarose hydrogel, our hybrid-hydrogel tape showed wider applicability to other noncovalent hydrogels as well.

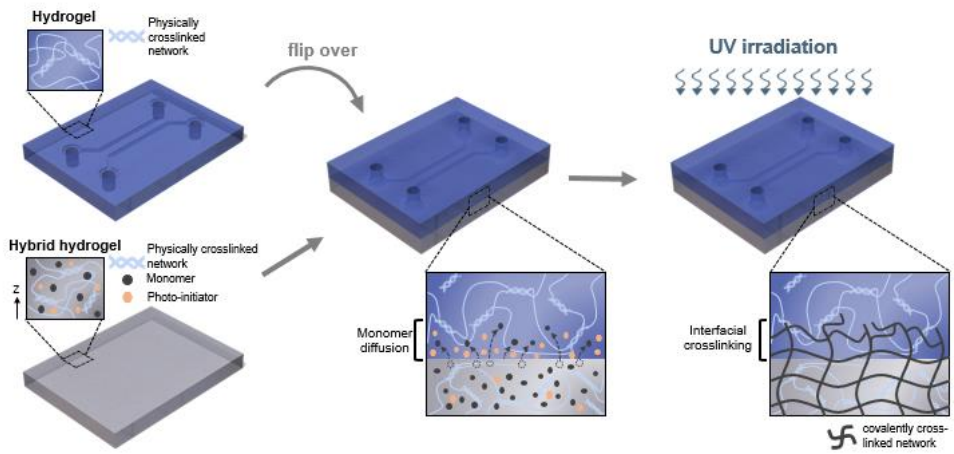

Figure 1. Schematic of noncovalent hydrogel to hybrid hydrogel bonding.

The bonding method requires no mechanical clamps and no bulk modification of the agarose hydrogel's polymer backbone. It is also compatible with preserving micropatterns within the bonding interface, unlike liquid glues. Our hybrid hydrogel consists of a physically crosslinked polymer network (aldehyde-activated agarose) embedded with UV-crosslinkable monomers (acrylamide, AAm) and initiator (APS or Irgacure 2959). The mechanism of bonding agarose hydrogel with this hybrid hydrogel is two-fold. First is 'network intertwining'. In detail, when agarose is placed on the hybrid hydrogel, this leads to passive diffusion of UV-crosslinkable monomers from the hybrid hydrogel into the noncovalent hydrogel matrix. After photo- or thermal polymerization, covalent network forms not only the second polymer network within the hybrid hydrogel but also the bonding interface that intertwines between agarose hydrogel and hybrid hydrogel.

The interpenetrating network (IPN) formed at the two hydrogels` interface was observable with SEM and EDS Second part of the mechanism is `network crosslinking` by Schiff base formation. When this bond formed between the hybrid hydrogel's aldehyde groups and amine groups within the interfacial layer's PAAm, the bonding strength was further increased compared to using 'network intertwining' alone. So due to the synergy of `network intertwining` and `network crosslinking` this single hybrid hydrogel was able to bond with various unmodified noncovalent hydrogels. The hybrid gel could also simultaneously covalently crosslink onto

elastomers and nonporous solids on its opposite surface using previously introduced solid surface treatments.

We also provide evidence that our bonding mechanism may be applicable to other noncovalent hydrogels such as agar, gelatin, alginate, and chitosan. With this new bonding technique, we were able to fabricate novel noncovalent hydrogel-solid integrated structures and functionalities.

As two big categories, the demonstrated applications of this bonding method could be divided into hydrogel microfluidics and single cell RNA analysis. For both side I relied heavily on agarose hydrogel. This was because the final and most important applications of both category were related to gel electrophoresis. It should be noted that although agarose is a widely accepted material for conventional gel electrophoresis, application of this material outside this technique was rather scarce. This was because, as mentioned before, is a noncovalent hydrogel incapable of strong bonding to other solid surfaces.

Due to the bonding method I introduce here, I expect to have broadened the potential of applying this material to other topics such as complex shaped microfluidics and hopefully, to tissue engineering, in which the potential of using agarose as scaffold material is being appreciated in recent years.

Chapter 2

Method of bonding noncovalent hydrogel to other hydrogels and solids

In this chapter, I introduce a generalizable bonding method that realizes interfacial bonding of noncovalent hydrogels to another tough, hybrid hydrogels without any glue or bulk modification of the noncovalent gel. As the noncovalent hydrogel contacts the hybrid hydrogel, the monomers within the hybrid gel passively diffuse into the noncovalent gel matrix at the interface. And by following photo-polymerization, the diffused monomers form cross-linked polymer networks within the noncovalent gel thus making the noncovalent gel fixed to the tough hybrid gel. This bonding method is generally applicable to many types of noncovalent gels including agarose, agar, gelatin, and sodium alginate.

2.1 Fabrication of hybrid hydrogel films

Otherwise stated, % means w/w%. For the agarose-AAm hybrid gel, a 10mL deionized water-based solution containing 19:1=AAm:MBAA solution at 5-40%, 0.05 w/v% APS, and 2mM $NaIO_4$ was degassed in a vacuum chamber for 15 minutes. A second deionized water-based solution containing 600mg agarose was heated in a microwave until agarose was fully dissolved with the final volume of 10mL and agarose concentration of 6%. The first mixture was poured into the second mixture and gently stirred until homogenous. 30uL of TEMED was then added to the mix, stirred gently until homogenous, immediately poured into ice-cold glass molds, and was put in a 4°C refrigerator for agarose gelation. When using Irgacure 2959, 0.2% Irgacure was used instead of APS the TEMED adding step can be omitted.

For the alginate-AAm gel, we referred to the previous publication with slight modification. Briefly, a 100mM Tris-HCl buffer-based 10mL solution containing 2% alginate, 12.05% AAm, 0.017% MBAA, 0.2% Irgacure 2959 (or 0.05 w/v% APS) was thoroughly degassed and quickly mixed with 20mM $CaSO_4$, 2mM TPP slurry and poured onto a mold. When using APS instead of Irgacure, the slurrry additionally contained 0.25 v/v% TEMED. The pregel was let to physically crosslink in a vacuum chamber for 10-60 minutes and then exposed to UV light ($14mW/cm^2$) for chemical crosslinking.

2.2 Fabrication of hybrid hydrogel and noncovalent hydrogel double layer structure

When using APS/TEMED based crosslinking**,** the bonding side of the agarose gel (1-3% agarose in either deionized water or 0.5x TBE buffer) was treated with benzophenone (10w/v% in absolute ethanol) for 1 minute and washed with absolute ethanol two times or until the surface is clear of benzophenone crystals. Remaining ethanol was removed and the surface was let at atmospheric condition until dry. Then it was transferred onto a hybrid gel and the assembly was exposed to UV irradiation for interfacial crosslinking (17mw/cm^2 for 15-30 minutes). When using Irgacure 2959 based crosslinking, no BP treatment was needed.

2.3 Performing various hydrogel-to-hybrid gel bonding

For agar hydrogel, mixture containing 3w/w% agar in deionized water was heated in a microwave until agar is fully dissolved. Then the mixture was poured onto glass mold and cooled at room temperature for gelation. For gelatin hydrogel, mixture containing 10 w/w% gelatin was heated in a microwave until agar is fully dissolved. Then the mixture was poured onto glass mold and cooled at room temperature for gelation. The gel was then submerged in glutaraldehyde solution (5 v/v% diluted in deionized water) overnight and then washed with deionized water. For alginate gel, pregel solution containing 2 w/w% sodium alginate was mixed to 100mM Tris-HCl buffer (pH 7.4) and dissolved by rotating the container overnight on a rotator (5rpm). The pregel solution was thoroughly degassed and mixed with a

slurry of containing ionic crosslinker (20mM $CaSO_4$) and crosslinking attenuator (2mM TPP), mixed until homogenous, poured into glass mold, and let to set in vacuum chamber for 1 hour. Before gelation, each pregel solution was mixed with food dye of designated color for final visualization.

Bonding each gel to hybrid gel was performed as same as agarose bonding to hybrid gel. Benzophenone treatment was omitted for negative control bonding samples.

2.4 Agarose hydrogel to tough hydrogel bonding procedure.

3% agarose gel was prepared as before but with an additional negative pattern. For tough hydrogel, 12.05% AAm, 0.017% MBAA, 2% sodium alginate, 0.05% APS was dissolved in 100mM Tris-HCl buffer (pH 7.4) solution by rotating the container, which was sealed to prevent light, overnight on a rotator (5rpm). The pregel solution was thoroughly degassed, mixed with a slurry for physical crosslinking (final concentration of 20mM $CaSO_4$, 2mM TPP) and 30-50uL of TEMED. Then the solution was mixed gently until homogenous, poured into the negative pattern on the agarose gel, and was let to solidify.

For the anti-fracture mechanism demonstration, pregel solution was poured into indentations of agarose gel molds and put under vacuum for 10 minutes for partial

physical crosslinking of the alginate. The entire agarose-tough pregel construct was exposed to UV light (17mW/cm^2, 60min) for chemical crosslinking.

For the self-aligned self-healing demonstration, we first poured the tough pregel solution into a silicon mold and let it in a vacuum chamber for a brief period for partial physical crosslinking and then placed a low melting agarose (LMA) film on top before exposing to UV light for chemical crosslinking.

2.5 Preparing solids and elastomers to bond with hybrid gels.

For glass or aluminum substrates, we adapted a previously reported TMSPMA-coating protocol[2]. Briefly, air plasma-activated glass, aluminum substrates were submerged in DI-based solution containing 1 wt.% TMSPMA, 0.1 v/v% acetic acid for 1-2 hours. The substrates were washed thoroughly with methanol and dried with air gun.

For PDMS substrates, PDMS film was air plasma-activated, treated with BP solution (10 w/v% in absolute ethanol), washed twice with methanol, and dried with air gun.

Chapter 3

Chemical validation of bonding technique

In this part, I produce results of a number of chemical measurements that validates my bonding technique. To be more specific, I performed FTIR experiments, NMR experiments, and other basic chemical reaction tests. FTIR measurements was performed to assess the chemical bonds present in various hydrogels including agarose, agarose:PAAm hybrid, and PAAm. The specific goal was to see whether imine bond is present in the hybrid film and not inside agarose or PAAm. NMR measurements was done to detect the aldehyde group occurring from sodium periodate treatment of agarose hydrogels. Also, to see if proper shifts occur compared to previously reported results of agarose and PAAm. SEM/EDS measurements was done to visually observe the monomer diffusion layer between the agarose and hybrid film. Other chemical tests were also performed as explained in the following chapter.

3.1 FTIR measurement of imine bond formation

3.1.1 Sample preparation for FTIR measurement

I prepared 3% agarose gel, PAAm gel, and agarose:PAAm hybrid gels. For the PAAm gel, 10w/v% AAm:MBA=19:1 in DI water was mixed with 0.015 w/v% APS, 0.15% TEMED and UV crosslinked with UV light (17mw/cm^2, 25minutes). Each gel was air dried in a ventilated hood overnight. The resulting dried films were used for FTIR absorbance measurement. FTIR spectra were recorded between 4000 and 400 cm^{-1} on a Thermo Scientific™ Nicolet™ iS™ 10 FT-IR spectrometer. The main focus was to detect the imine bond that should specifically appear in the hybrid hydrogel and not polyacrylamide or aldehyde-agarose sample.

3.1.2 FTIR Measurement result

FT-IR analysis of hybrid hydrogels with varying '$NaIO_4$ treatment duration' showed that with increasing duration, the imine (C=N, 1565cm^{-1}) peak of schiff-base increased while the amide II (1565cm^{-1}) peak of PAAm chain decreased. This indicated that PAAm amides were being consumed to form imine bond with aldehyde groups on the agarose chain, thus confirming our hypothesis.

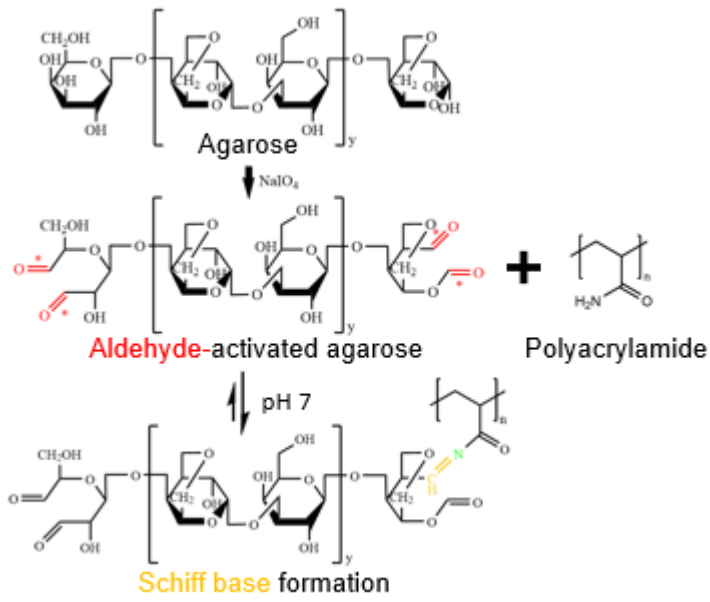

Figure 2. Description of agarose aldehyde activation and forming imine bond (Schiff base) with polyacrylamide chain

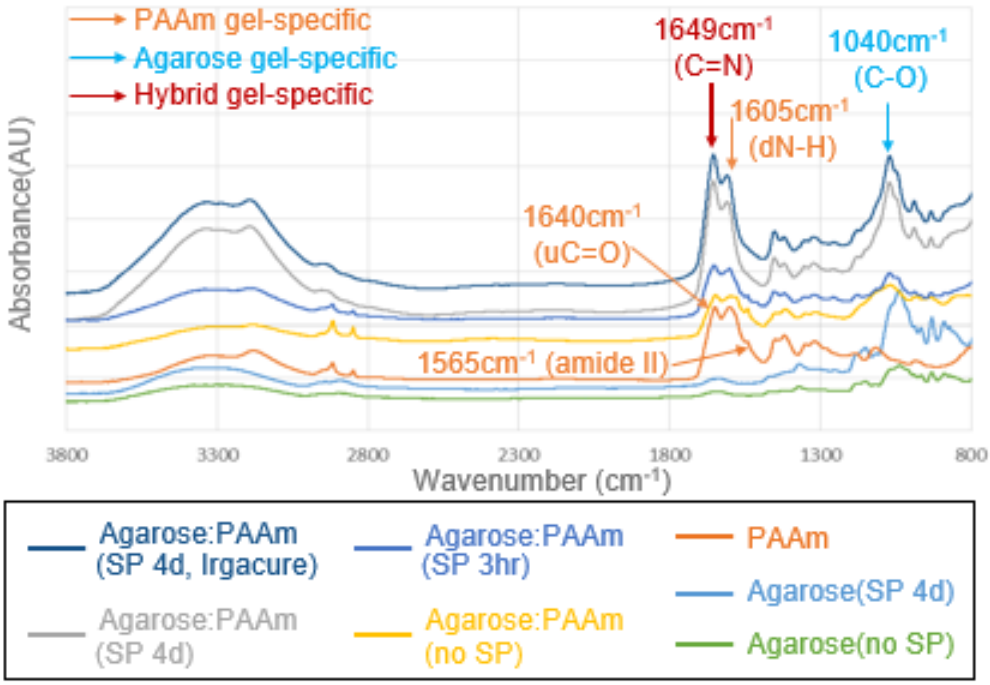

Figure 3. FT-IR measurement result. The C=N bond was specifically increased in the hybrid hydrogel sample. SP: sodium periodate. PAAm: Polyacrylamide. 4d: 4-day treatment

3.2 13C-NMR chemical shift measurement

3.2.1 Sample preparation for NMR measurement

As the NMR machine only works well for liquid state samples. We had to perform heated NMR at around 60°C to prevent the agarose sample from solidifying. Also, as imine bond does not form under such high temperature conditions, we were only able to measure the aldehyde groups formed by sodium periodate treatment. Agarose activation was conducted by first suspending agarose powder in DI water containing 1-20mM of sodium perdioate. The mixture was sealed to protect from light and stirred gently at room temperature for various duration (from 3 hours to several days). The resulting activated agarose powder was washed with DI water several times.

Sodium-perdiate-treated agarose, bare agarose and Irgacure2959 mixed in pure deuterium water. The samples were preheated and immediately mounted into an NMR machine with ^{13}C mode. In more detail, nuclear magnetic resonance chemical shifts were measured by a 600MHz, high resolution NMR spectrometer (AVANCE 600, Bruker). Hybrid gel samples were prepared in D_2O with the identical composition (agarose, acrylamide, photoinitiator) as the hybrid gels used for tensile test except MBAA which was removed to prevent excessive gel crosslinking.

Agarose gel and polyacrylamide gel samples were prepared in D_2O with 3% (w/w) and 5% (w/w), respectively. All samples contained either 0.2% Irgacure 2959 or 0.15% TEMED and 0.25% (w/v) and were exposed to UV irradiation (254nm,

14mW/cm^2, 25min). Samples that contained agarose were boiled to completely melt the gel and was heated to 60°C during NMR measurements.

3.2.2 NMR measurement result

I also performed NMR spectrum prediction using an online-available program and mol file and the peaks to see if it shows high correlation with the actual agarose result. The NMR shifts of the experiment result closely resembled that of the peaks predicted by simulation. The simulation was based on the chemical structures of agarose chain given by the user.

Compared to natural agarose, most of the shifts were identical for the $NaIO_4$-treated agarose. However for $NaIO_4$-treated agarose, it contained an additional 210 ppm peak which corresponded to the carbonyl group of the aldehyde group. This was as I expected since there are no carbonyl groups in conventional agarose. Also, the NMR pattern of hybrid hydrogel showed the superposition pattern of PAAm and agarose as expected. I did this experiment to see whether imine bond expected to have formed between the PAAm chain and the aldehyde-agarose chain could be observable. However, the imine bond was not observable in the NMR result. This probably could be caused by the high temperature treatment needed during the NMR measurement.

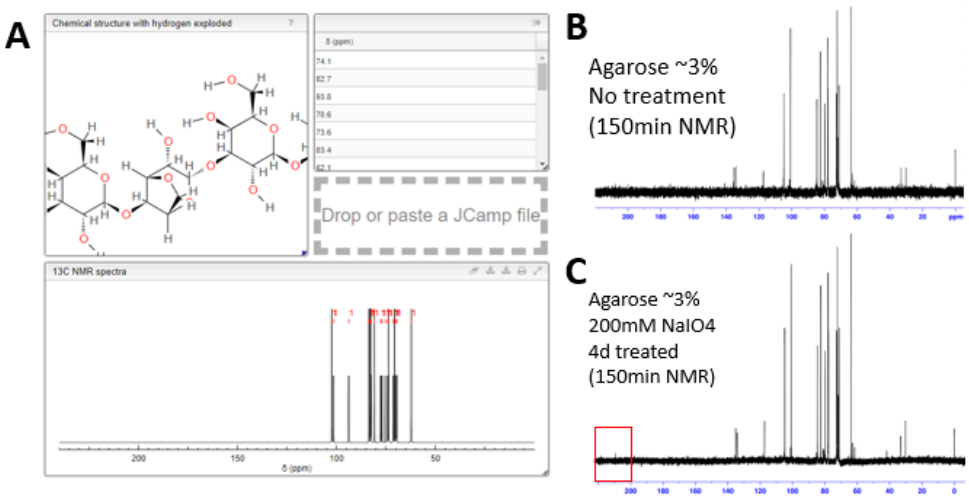

Figure 4. Agarose and aldehyde-agarose NMR measurement simulation and actual result. A shows the simulation result based on agarose chain structure. B,C each shows the actual NMR shift spectrum of normal agarose and aldehyde-activated agarose. The red box in C shows the aldehyde peak.

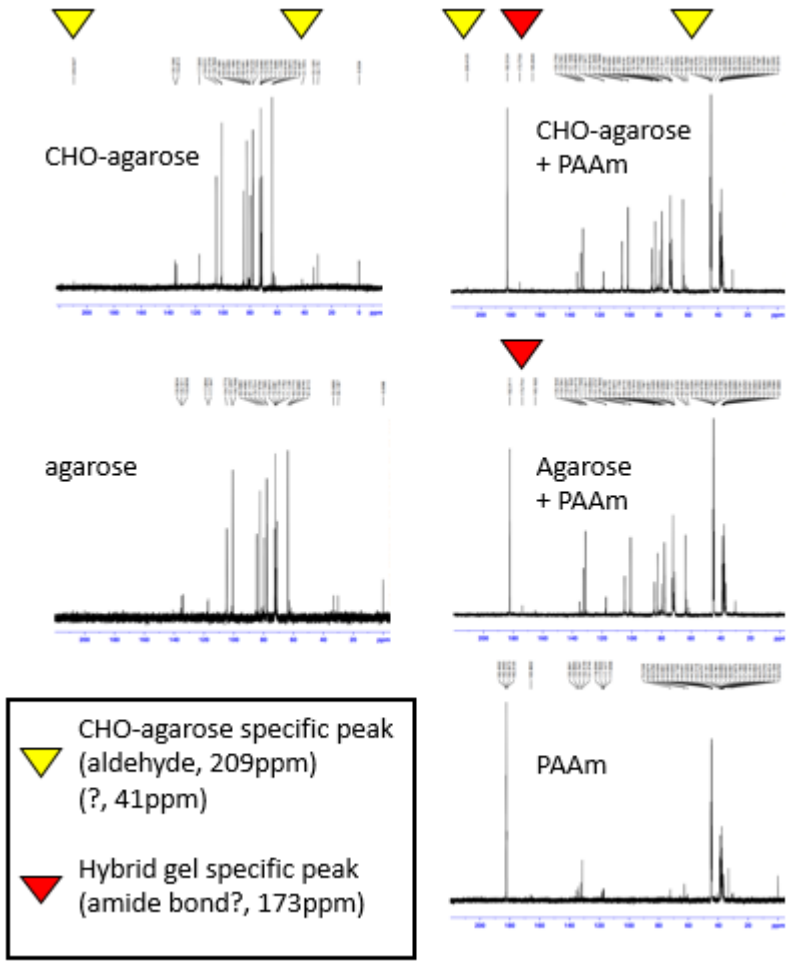

Figure 5. Comparison of hybrid gel NMR peaks with peaks from agarose, aldehyde-agarose and PAAm. Yellow triangles indicate aldehyde-agarose specific peaks including the 209 ppm peak. Red arrow indicates the hybrid gel specific peak.

3.3 SEM/EDS measurement of monomer diffusion layer

3.3.1 Sample preparation for SEM measurement

To further verify our hypothesis of interfacial network formation, we imaged the cross-section between agarose gel and tough agarose gel with scanning electron microscopy (SEM). For this we prepared agarose hydrogel:hybrid hydrogel double layers with dimension of approximately 20 x 50 x 4 mm. The bonding procedure was as before. We then sliced the slab into thin, 2mm slices, each containing a agarose:hybrid bonded structure. We transferred these thin slices into liquid nitrogen for snap-freezing. We transported the sample to a facility and freeze-dried in a -110°C quick freeze-drying chamber overnight or for 2-3 days until the samples were fully dry. As soon as the samples were fully dried, we transferred to a SEM facility and were treated with platinum coating. Then the samples were then mounted into a SEM device.

3.3.2 SEM measurement result

The 200x image of the cross section revealed a clear interface (thickness of around 300um) formed between the agarose gel and tough agarose gel. SEM imaging showed clear separation of 3 layers. From top to bottom they were agarose hydrogel, intermediate region, and hybrid hydrogel. The intermediate region had a varying thickness but on average the thickness was around 100-300um. We tried both APS/TEMED hybrid hydrogels and Irgacure2959 hybrid hydrogels. Both showed

similar intermediate region occurring.

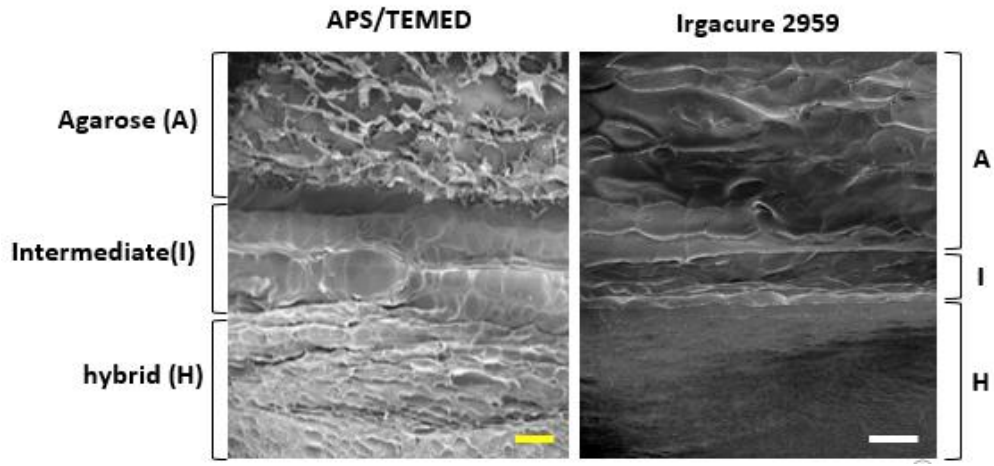

Figure 6. SEM image of the agarose/hybrid gel intermediate.

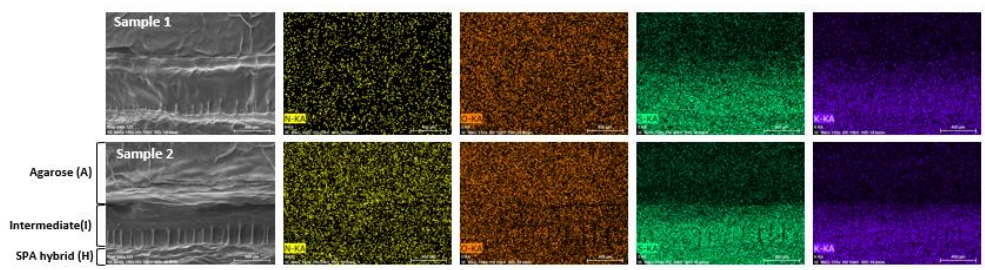

Figure 7. **. EDS image of the agarose/hybrid hydrogel interface.** From left to right is the original SEM image, Sodium (N), Oxygen (O), Sulfur(S), Potassium (K) image. Each row are images from the same sample.

3.3.3 EDS measurement result

A 10mL deionized water-based solution containing 0.63% MBAA, 12% AAm (or 40% SPA-K), 0.2% Irgacure 2959, and 2mM $NaIO_4$ was degassed in a vacuum chamber for 15 minutes. A second deionized water-based solution containing 600mg low melting agarose was heated in a microwave until agarose was fully dissolved with the final volume of 10mL and agarose concentration of 6%. The first mixture was poured into the second mixture and gently stirred until homogenous. The solution was poured into ice-cold glass molds, and was put in a 4°C refrigerator for agarose gelation. The agarose-hybrid gel composite was prepared as explained above. Then the composite was sliced into 1-2 mm thick slices and freeze dried in a -110°C freeze-dryer overnight. SEM imaging and EDS measurement was conducted using a FESEM Auriga (Zeiss Inc.) machine.

AAm diffusion from tough gel to agarose gel will not lead to bulk modification of the agarose gel network. So we hypothesized that AAm diffusion would be rather limited to the interface of agarose gel and tough gel and form interfacial interpenetrating networks when exposed to UV light.

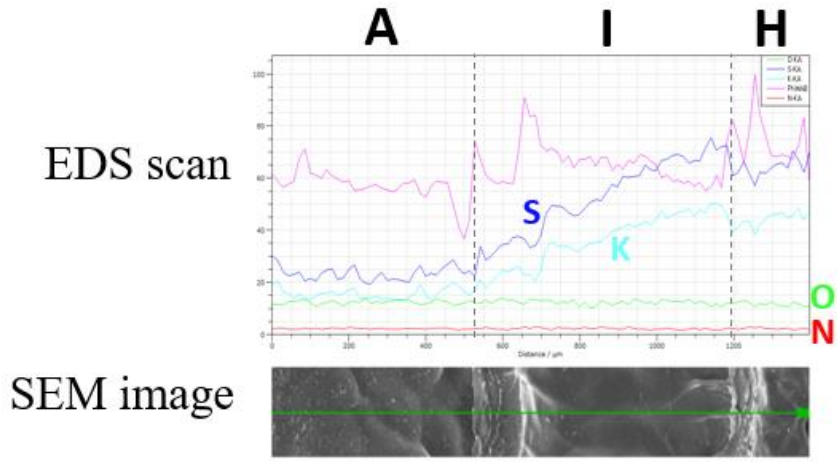

Figure 8. EDS line scanning data. The EDS scan was done on the SEM image (below) along the given arrow line. From hybrid (H) to agarose (A), along the intermediate region, the Sulfur (S) and Potassium (K) concentration reduced gradually while O, N concentration didn't vary.

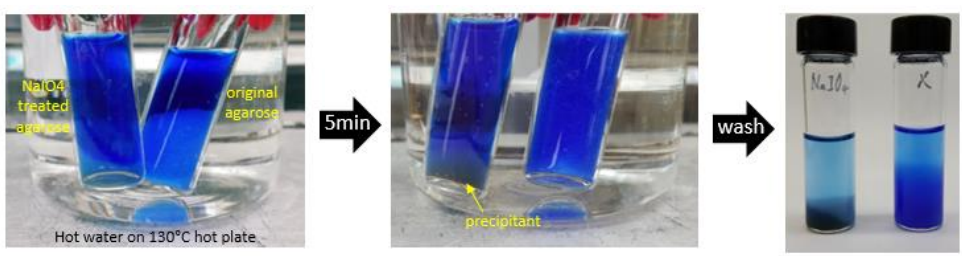

Figure 9. Fehling test based verification of aldehyde-agarose. Only the sodium periodate-treated agarose produced precipitant after reaction.

To definitively prove our hypothesis of the bonding mechanism, we devised an EDS experiment to see if the crosslinkable monomers indeed diffused into the agarose gel matrix. To discriminate the monomers from neighboring agarose matrix, we substituted acrylamide with sulfoxypropyl acrylamide-potassium salt (SPA-K) which contains high molecular weight sulphur and potassium. We expected that if the monomers diffused into the agarose gel and then form polymers, the EDS signal of SPA-K should be saturated within the hybrid gel, penetrate through the agarose gel while steadily decreasing in intensity with depth. SEM image of the agarose-hybrid bonding interface revealed a third, morphologically distinct intermediate layer with uniform thickness possibly formed by the diffused monomer. EDS profile, as expected, showed sulphur and potassium signal (from SPA-K) diffusing from hybrid gel into the intermediate layer and remaining base level throughout the pure agarose gel layer. In contrast, signals of oxygen and nitrogen was uniform across the three layers. This result definitively proved our bonding mechanism is based on interfacial IPN formation by diffused monomers.

I also performed Fehling test to verify the effects of sodium periodate. For this, 0.9g of agarose powder was treated with 20mL of 0.2M $NaIO_4$ solution (in DIW) for 4~5 days with vertical rotation at 20rpm. Equal volume (5mL) of Fehling solution A and B were pre-mixed. 5ml of Fehling solution was added to pure agarose powder or $NaIO_4$-treated agarose powder (in glass containers) The samples were submerged

in hot water for 5 minutes. The result showed that only the NaIO4-treated agarose sample produce reddish precipitant appearing. This verified that NaIO4-treated agarose samples have aldehyde groups activated, probably at the chain ends.

Conclusively, we demonstrated an adhesive-free noncovalent gel to tough gel bonding protocol and verified its mechanism, which is formation of UV-induced thin, strong IPN network at the interface.

Chapter 4

Bonding performance analysis

In this chapter, I present the results of a number of tensile tests based bonding performance analysis. The bonding strength between noncovalenet hydrogels, especially agarose, and the hybrid film was measured with varying conditions. Flatwise tensile test was used as the principle method, for which I designed a custom holder setup. The parameters that were assessed were monomer concentration within the hybrid film, sodium periodate treatment concentration for the agarose chain within the hybrid film, and monomer diffusion time. I also analyzed the debonding characteristics using extension-force curve analysis and fracture energy measurement tests.

4.1 Bonding strength measurement

4.1.1 The effect of monomer concentration

To measure the bonding strength between a typical noncovalent hydrogel and hybrid hydrogel, we bonded agarose gel with agarose-acrylamide(AAm) hybrid hydrogel and performed flatwise tensile test.

For this we designed a custom zig made with aluminum plates and bolts. The hydrogel parts were first attached to a custom acrylic plate with fast glue. This ensures the hydrogels do not detach from the zig even with high bonding strength between agarose hydrogel and hybrid hydrogel. So both side of an agarose:hybrid hydrogel construct was bonded with acrylic plates. Then the acrylic plates were fixed to the aluminum zig with a constraining aluminum bar with nut and bolt joining. I gave 5 minute incubation time for the fast glue to fully polymerize, before tensile test initiation. The construct was put under flatwise tensile test with extension speed of 10mm/min, the minimum value available. I also made sure that the bonding area between agarose and hybrid hydrogel was 25 x 25 mm by inserting a PET film or glass film as a spacer with a square hole in the middle with the indicated dimension before UV based bonding.

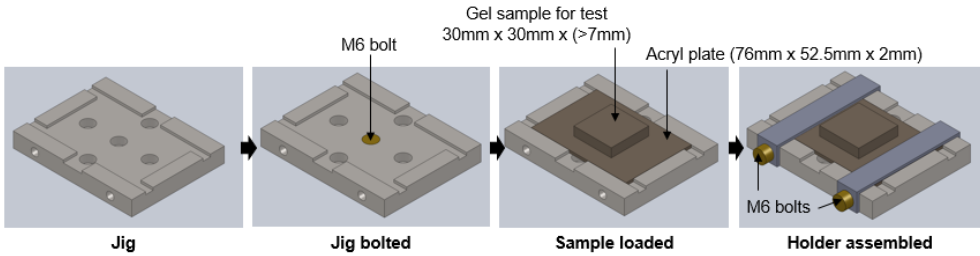

Figure 10. Jig design and sample preparation procedure. The jig is first bolted to the tensile tester using an M6 bolt. Then the hybrid gel or noncovalent hydrogel-bonded acryl plate is placed on the jig. Then a pair of fixing plates are bolted to the jig using M6 bolts.

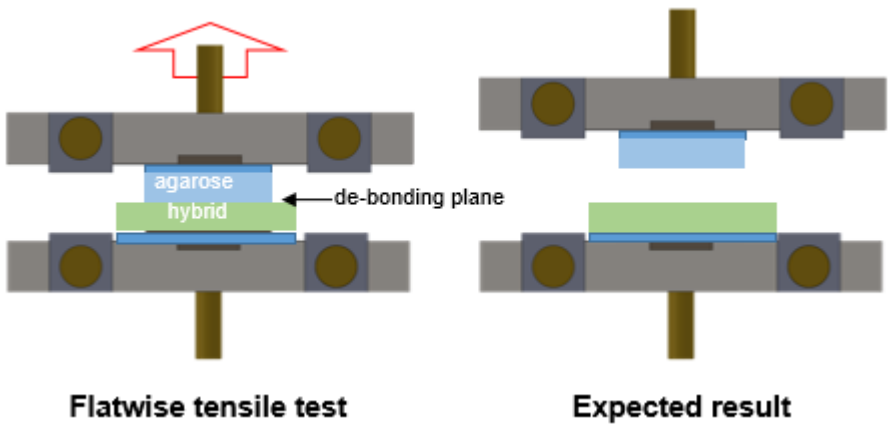

Figure 11. Flatwise tensile test example schematic. The additional jig for the upside hydrogel is pre-assembled with an acryl plate that has been painted with fast glue and is carefully let to contact the upside hydrogel and let to fix for > 1 minutes. Then the actual tensile test is perforemed.

I hypothesized that AAm monomer concentration within the hybrid hydrogel will affect the bonding strength, since with increasing monomer concentration will lead to denser PAAm intertwining within the intermediate region. As expected, I observed dose dependency of adhesive failure between agarose hydrogel and agarose:PAAm hybrid hydrogel containing 5~15 w/v% AAm:MBA=19:1 concentration. This indicates that at this AAm concentration , the bonding strength doesn't exceed the cohesive force of agarose chains within the agarose gel matrix. Beyond 15 w/w%, cohesive failure occurred due to the interface bonding strength exceeding the cohesive strength of agarose gel.

The force-extension curves of these experiments showed that adjusting AAm concentration within hybrid hydrogel changed the modulus of the construct. This can be seen as the slope of the force-extension curve increasing with increasing monomer concentration. The area under the curve also increased with monomer concentration, indicating increase in toughness.

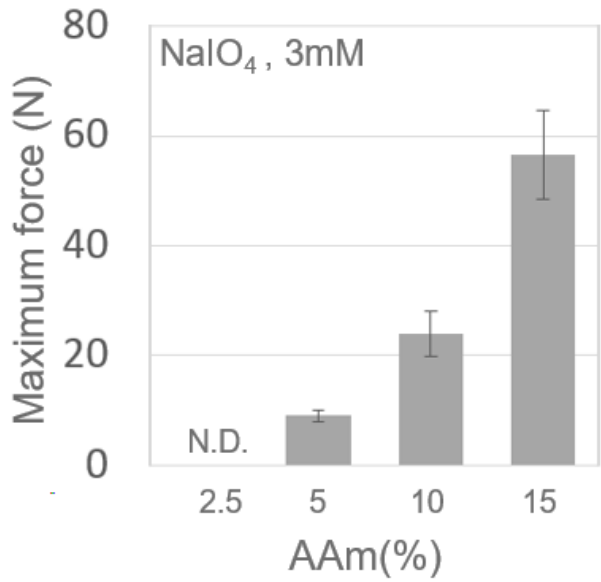

Figure 12. Bonding strength measurement with varying AAm monomer concentration within hybrid hydrogel. Sodium periodate treatment condition (3mM) was the same for all samples.

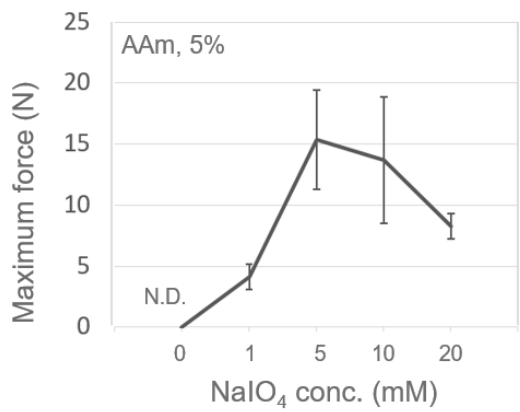

Figure 13. Bonding strength with varying sodium periodate concentration.

4.1.2 The effect of agarose chain aldehyde modification

Additionally, beside the monomer concentration, I discovered that bonding strength could be further increased by adjusting the aldehyde-activation level of agarose chain within the hybrid hydrogel. This aldehyde-activation was conducted by treating agarose powder with varying concentrations of oxidative sodium periodate ($NaIO_4$). For this I treated the agarose powder with varying sodium periodate concentration with a fixed duration. Sodium periodate was washed out and the resulting agarose powder was melted by heat and mixed with a fixed concentration of AAm and initiator to prepare hybrid films and bonded with agarose hydrogel as previous sections. The resulting flatwise tensile test

To further analyze the result, I analyzed the raw force-extension curve in more detail. In other words, I observed the slope of the force-extension curve during the tensile test up to the point of actual debonding. This is important since the slope dynamics during the tensile test gives information of the material characteristics such as toughness of the bond, toughness of the material, modulus of the material and so forth. For example, if the slope increases, it means increase in modulus. If the total extension increases even with the same maximum force before debonding, it indicates increase in stretchability. If the overall area under the force-extension curve increases, it indicates increase in toughness.

The force-extension curves of these experiments showed that adjusting aldehyde activation within the hybrid's agarose network changed the stretchability

of the construct. This can be seen as the force-extension curve having similar slope despite the variation in maximum force with different sodium periodate treatment strength. Specifically, the maximum force reached peak value with 5mM sodium periodate treatment. The reason of the maximum force, or the stretchability, decreasing after further sodium periodate concentration was unexplainable with our knowledge.

However, fact remains that the imine bond occurring within the hybrid film during bonding has a positive effect for the bonding strength. This could be explained that the intertwining PAAm network within the intermediate region can be chemically anchored to the underlying hybrid gel's aldehyde-agarose chain, thus having increased resistance against disruptive debonding force. Although bonding between hydrogels with a diffusive monomer is a previously known method to produce bonding effect, this sodium periodate-based anchoring is, to our knowledge, a novel approach.

4.1.3 The effect of monomer diffusion

Maximum force measured with varying monomer diffusion time. hybrid gel contained 3% agarose activated with 24 hour treatment of 100mM $NaIO_4$, 10% (w/v) AAm:MBA=19:1, 0.2% Irgacure 2959. The duration of monomer diffusion showed no significant effect on the bonding strength.

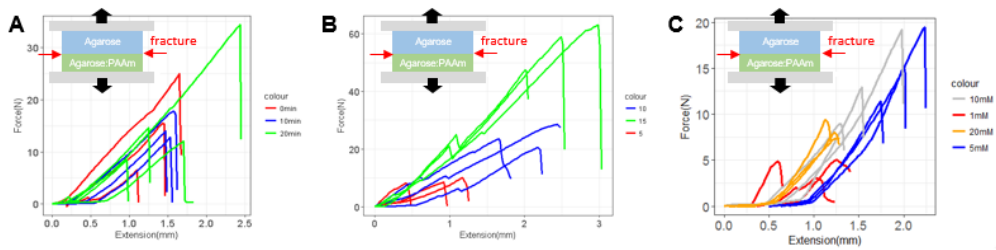

Figure 14. Raw extension-force curves for diffusion time variation (A), AAm concentration variation (B), and sodium periodate treatment concentration variation (C).

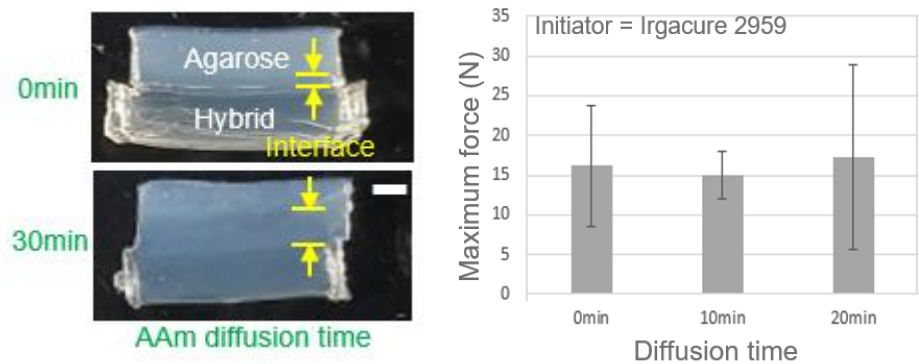

Figure 15. **AAm diffusion time variation bonding strength effect test.** Left shows images of the varying intermediate region thickness with different diffusion time. Right shows the bonding strength with varying diffusion time.

When I perform tensile test on agarose:hybrid, the debonding plane doesn't occur within the interface region but either at i) the original agarose gel and hybrid contact plane (Case 1 and 2) or ii) within the pure agarose gel part (Case 3). So the interface thickness has no effect on the bonding strength (=the ultimate force measured at the point of fracture).

4.1.4 Fracture energy analysis

Was shown above, the raw force-extension curves of the varying sodium periodate concentration experiment shows that only the stretchability not the modulus of the bonded structure is varied. I hypothesized that the sodium periodate concentration variation might affect the fracture energy (stretchability) of the hybrid hydrogel itself. However, fracture energy measurement experiment showed that sodium periodate concentration does not affect the stretchability of the hybrid hydrogel. Therefore, the stretchability of the agarose:hybrid bonded structure indeed comes from the interface stretchability.

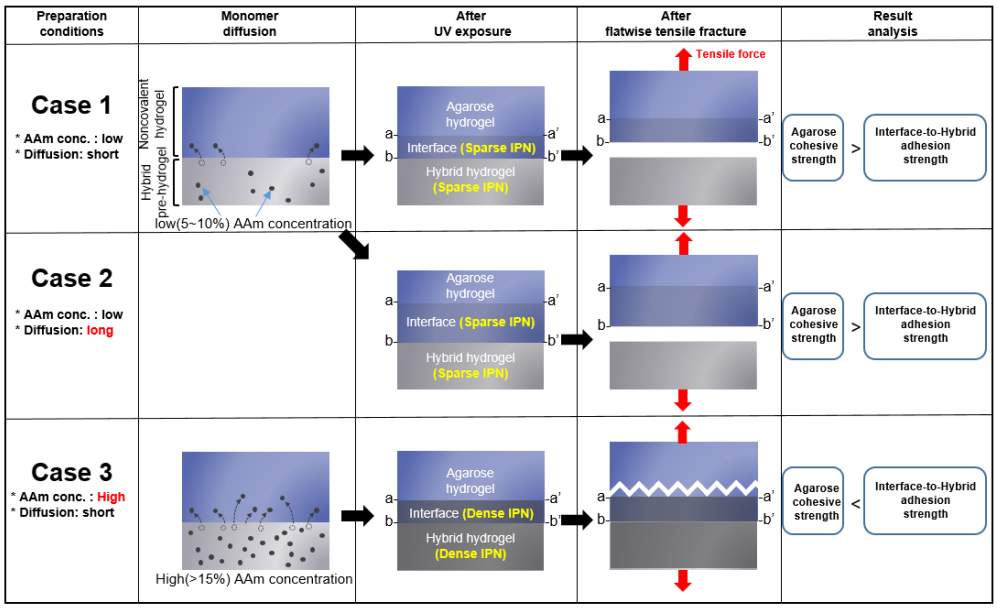

Figure 16. **Schematic explanation of the reason why diffusion time did not affect bonding strength.** The debonding plane was always the plane between the agarose and hybrid hydrogel original contact surfaces, regardless of the monomer diffusion layer thickness or monomer concentration.

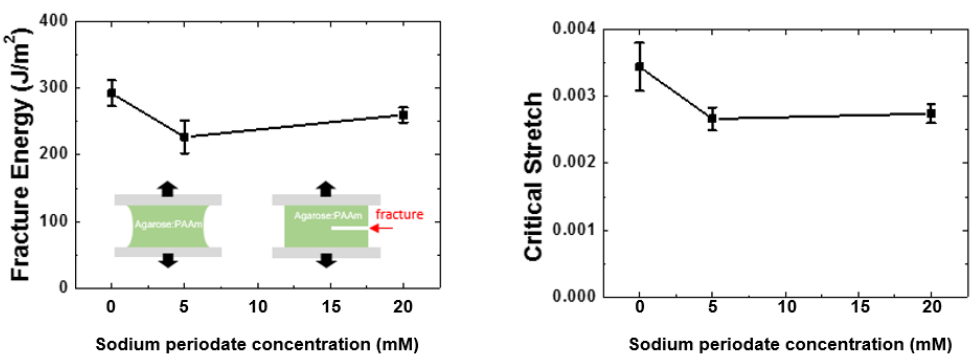

Figure 17. **Fracture energy measurement of hybrid hydrogel.** Sodium periodate concentration did not affect fracture energy of the hybrid hydrogel.

4.2 Noncovalent hydrogel to solid bonding

4.2.1 Noncovalent hydrogel to solid surface bonding

Based on these results, I expanded the spectrum of this noncovalent hydrogel bonding method to bonding with solid materials. First, I bonded noncovalent agarose gel with oxide-containing solid materials by using our hybrid hydrogel as a two-sided tape. We designed a 5 layer construct (glass-hybrid-agarose-hybrid-aluminum) that was bonded together by a single UV exposure step.

I first demonstrated strong bonding of agarose gel to either TMSPMA-coated glass or TMSPMA-coated aluminum using our hybrid hydrogel films as interface. The construct consisting of 5 layers (glass-hybrid-agarose-hybrid-aluminum) was created by simply overlaying each layer and exposing with a single UV exposure step, demonstrating the simplicity of our method.

The resulting construct (bonding area=25mm x 30mm) was able to withstand a shear force of 3kgf. The bonding mechanism between TMSPMA-coated solid and hybrid gel is simple radical crosslinking between acrylate functional groups.

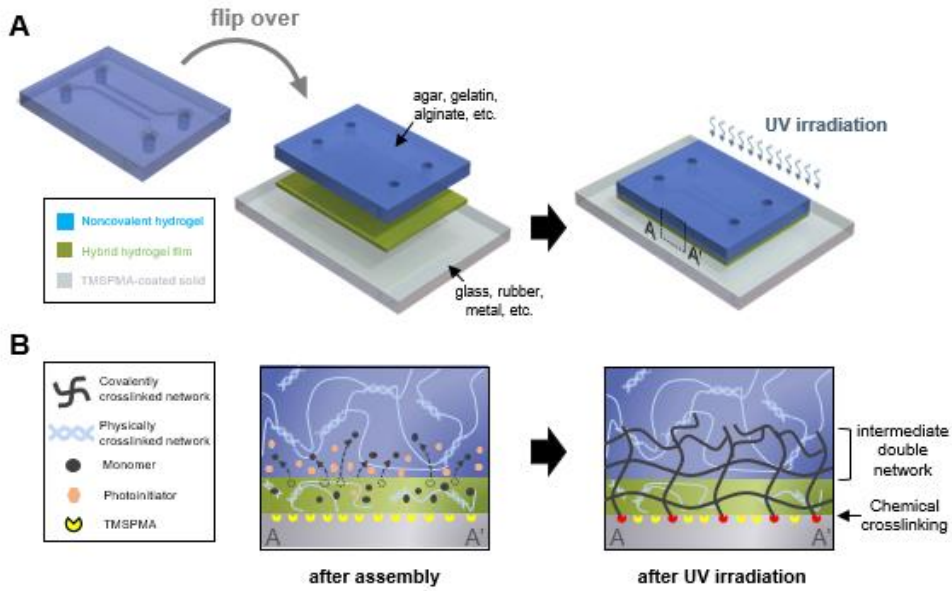

Figure 18. **Schematic of noncovalent hydrogel to solid surface bonding.**

4.2.2 Noncovalent hydrogel to elastomer surface bonding

These results clearly supported my hypothesis that monomer diffusion and subsequent double network formation is the basis of my noncovalent gel to tough gel bonding mechanism. I suspected that the intermediate layer thickness would reduced as AAm or SPA-K concentration is lowered in hybrid gel, although I weren't able to verify this because lower monomer concentration caused significant debonding and fracturing during freeze-drying (data not shown).

It is still possible that agarose gel and hybrid gel bonded due to reversible sol-gel process. In other words, since both gel contains agarose exothermic UV curing could have triggered agarose gel-sol process followed by sol-gel process that now binds the two agarose matrices. To reject this possibility, I decided to investigate whether one can bond a noncovalent hydrogel with distinct material from the hybrid gel.

Consequently, I decided to assess whether the suggested bonding method can be applied to other noncovalent hydrogels such as gelatin, agar, chitosan and alginate. These hydrogels have different polymer backbone but still form hydrogel with hydrogen bond like agarose. I also decided to perform noncovalent hydrogel to elastomer bonding with the same hybrid film.

For agar hydrogel, mixture containing 3w/w% agar in deionized water was heated in a microwave until agar was fully dissolved. Then the mixture was poured onto glass mold and cooled at room temperature for gelation. For gelatin hydrogel, mixture containing 10 w/w% gelatin in deionized water was heated in a microwave

until gelatin was fully dissolved. Then the mixture was poured onto glass mold and cooled at room temperature for gelation. When internal crosslinking was needed, the gel was then submerged in glutaraldehyde solution (5 v/v% diluted in deionized water) overnight and then washed with deionized water. For alginate gel, pregel solution containing 2 w/w% sodium alginate was mixed to 100mM Tris-HCl buffer (pH 7.4) and dissolved by rotating the container overnight on a rotator (5rpm). The pregel solution was thoroughly degassed and mixed with a slurry containing ionic crosslinker (20mM $CaSO_4$) and crosslinking attenuator (2mM TPP). Immediately, the solution was mixed until homogenous, poured into glass mold, and was let to set in vacuum chamber for 1 hour. To visually discriminate different gels, each pregel solution was mixed with food dye of designated color.

Since these noncovalent hydrogels are extremely fragile, we assess the bonding result by a simple bending test using thin PDMS films as solid backing. The three layer (gel-hybrid-PDMS) composite was prepared similarly with the 5 layer experiment before, except that the PDMS film was treated with benzophenone instead of TMSPMA (see materials and methods). For elastomer bonding, so I choose PDMS. PDMS films with 1mm thickness was prepared by pouring degassed PDMS:sylgard184=10:1 solution in glass mold and curing at 90°C for 1 hour. Bonding side of the PDMS films were treated with benzophenone (10 w/v% in absolute ethanol) for 1 minute and washed with methanol 2 times. Hydrogel-hybrid-

PDMS was sequentially stacked and bonded by simply exposing to UV (17mw/cm^2, 15 minutes). For negative controls, the hydrogel was stacked onto a pre-UV-exposed (17mw/cm^2, 5 minutes) hybrid-PDMS composite and was exposed to UV (17mw/cm^2) for additional 10 minutes.

I was successful in producing higher bonding strength, compared to simple adhesion, between agarose:PAAm hybrid hydrogel and other noncovalent hydrogels such as agar, alginate and gelatin. Similarly, I also succeeded in bonding noncovalent hydrogels to hydrophobic PDMS slabs pretreated with benzophenone. The control experiments were, in detail, noncovalent gels loaded on a pre-UV crosslinked hybrid-PDMS composite. They were not able to maintain adhesion during bending. This shows that our method creates stronger bonds than weak adhesion force, which is surprisingly often used for in vitro assays using noncovalent gel-solid constructs.

In exception, gelatin is well known to have high adhesion force to various solid surfaces by reversible thermal sol-gel process.Ie also noticed that gelatin tends to melt by the moderate heat generated during UV exposure and subsequently tightly binds to the underlying solid substrate by gelation after cooling.

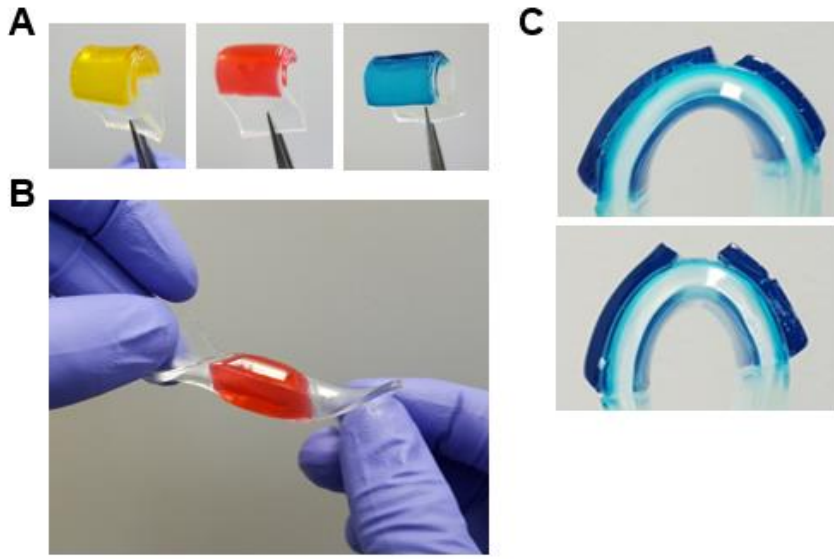

Figure 19. **Bonding hybrid hydrogel with various noncovalent hydrogel.** In A, from left to right is alginate, gelatin, and agar hydrogel bonded to hybrid hydrogel slab. B shows the high bonding strength of gelatin to hybrid hydrogel. C shows the fracture of agar gel after bending test yet remaining bonded.

To exclude the possibility that gelatin was bonded by this nonspecific adhesion force, I first crosslinked the gelatin matrix with glutaraldehyde to prevent thermal denaturation .When using this crosslinked gelatin for bending test, bonding succeeded only when AAm monomers from the hybrid layer diffused into the gelatin matrix before UV exposure and a crosslinked gelatin was not able to bond onto pre-UV-crosslinked hybrid gel. This demonstrated that the monomer diffusion and subsequent interfacial crosslinking mechanism is the dominant factor for gel bonding for every naturally derived hydrogels tested.

Therefore, my noncovalent hydrogel-hybrid hydrogel bonding mechanism is not based on thermal or ionic gelation which works in bonding hydrogels with identical gelling mechanism (e.g. hydrogen bonding, ionic bonding). It also differs from previous chemical hydrogel-to-hydrogel bonding method where both hydrogel parts had to contain crosslinkable monomers.

4.2.3 Noncovalent hydrogel to tough hydrogel bonding

For the anti-fracture mechanism demonstration, alginate-AAm pregel solution was poured into indentations of agarose gel. The construct was put into a vacuum chamber for 10 minutes for partial physical crosslinking of alginate. The entire agarose-tough pregel construct was exposed to UV light (17mW/cm^2, 60min). For the self-aligned gel healing demonstration, we first poured the pregel solution onto an ecoflex film and let it in a vacuum chamber for 1 minute for partial physical

crosslinking and then placed a low melting agarose (LMA) film on top before exposing to UV light for chemical crosslinking.

With the proposed bonding method I also performed an anti-fracture mechanism. By bonding an agarose slab with the tough hydrogel anchor, one could perform a fracturable yet stretchable hydrogel structure mechanism. I also was able to perform a self-aligned self-healing mechanism. For conventional self-healing mechanisms, the alignment step must be done manually. Without the alignment, self-healing could not happen. However, I could perform the self-healing step even without the manual alignment. This was because the agarose hydrogel was attached to the tough, stretchable hydrogel which was bonded to an elastic elastomer. For this bonding to happen, the TPP was necessary to delay the gelling process of the tough hydrogel. Without the TPP treatment, the monomers within the tough hydrogel pregel solution was not able to diffuse into the agarose hydrogel for intermediate region formation.

In conclusion, I verified that my bonding mechanism is based on intermediate crosslinking and not reversible sol-gel process. The results also showed that my hybrid gel film is a versatile intermediate that can enable bonding various noncovalent hydrogels to solid materials. With additional experiments, I also found that the bonding mechanism still works when agarose within the hybrid gel is replaced with alginate.

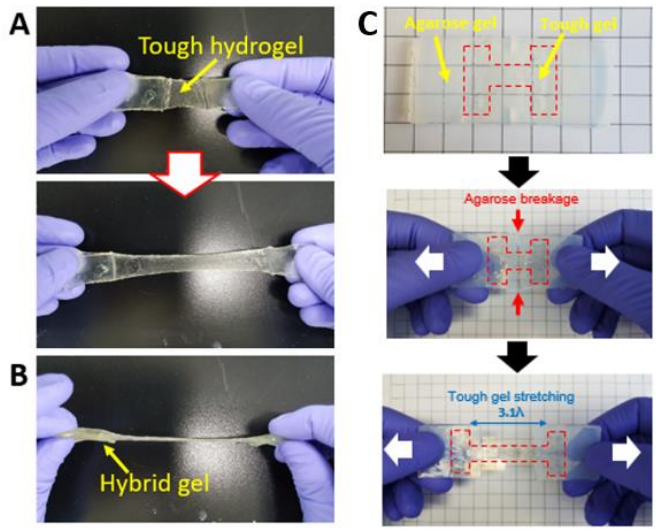

Figure 20. **Bonding tough hydrogel with hybrid hydrogel or noncovalent hydrogel.** A and B shows bonding tough hydrogel bonded to hybrid hydrogel. C shows a dumbbell shaped tough hydrogel bonded to a slab of agarose hydrogel. For C, the bonded structure showed stretchability of around 310% before debonding between agarose and tough hydrogel.

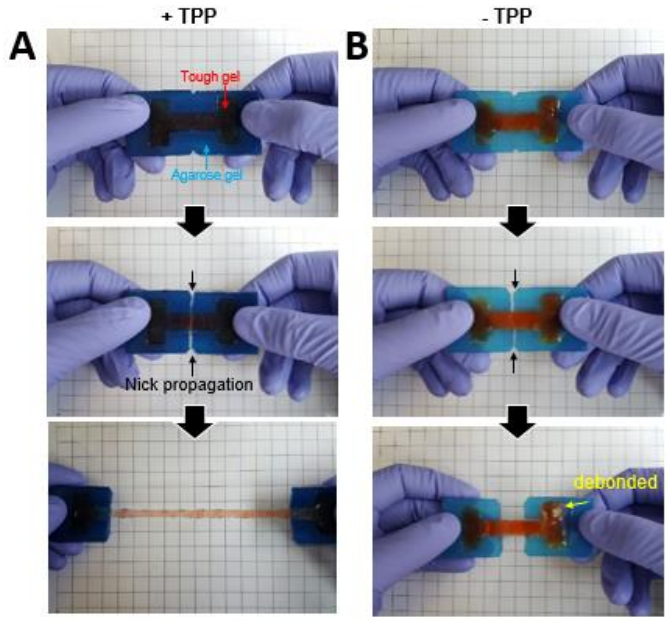

Figure 21. **Bonding tough hydrogel with agarose hydrogel in the presence or absence of TPP treatment.** TPP treatment was critical for successful bonding between tough hydrogel and agarose hydrogel.

Chapter 5

Demonstration of application

In this chapter, I demonstrated a microfluidic hydrogel system. Unlike previously introduced agarose based microfluidic chips, the presented demonstration did not need any liquid glue or mechanical jigs for fixation. This was due to the bonding technique introduced above. Since the hybrid hydrogel film acts like a two-sided tape that preserves interfacial micropatterns, this bonding technique was optimal for high flow rate microfluidics and non-planar, curved microfluidic systems.

5.1 Zig-free hydrogel microfluidic system

As mentioned before, the technique of patterning microstructures between noncovalent hydrogel and solid interface is highly useful for many in vitro assay experiments. Unfortunately, when using micropatterned agarose gels, previous works mostly relied on weak adhesion force or bulky mechanical anchorages to seal the micropatterns and keep gel to solid attached.

But adhesion force cannot withstand high flow rate or high internal pressure (e.g. fluidic pressure in microchannel). And mechanical anchorage limits scalability of the system. Previously, fabricating a robust noncovalent hydrogel-based microfluidic system required mechanical anchorage between microchannel-patterned hydrogel and solid surface, thus limiting scalability and design flexibility.

In contrast, my bonding mechanism is capable of robustly sealing microchannels while no mechanical anchorage is required to maintain gel to solid attachment. I was able to robustly bond microchannel-patterned agarose gel onto glass substrates without mechanical anchorage.

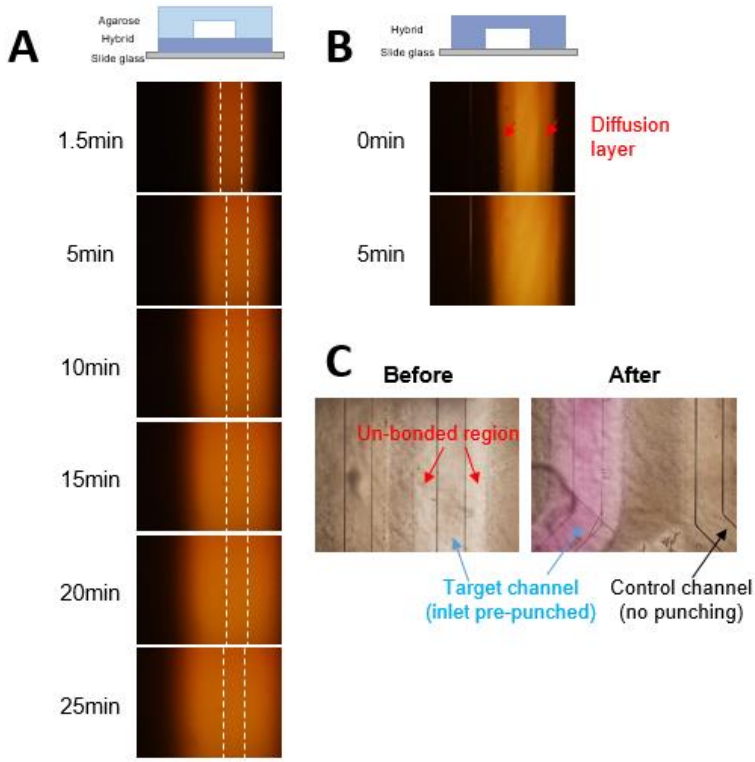

Figure 22. **Diffusive agarose microfluidic system without mechanical jig fixation.** A shows the diffusive flow of Rhodamine B solution in a micropatterned agarose hydrogel system. B shows the diffusive flow of Rhodamine B solution in a micropatterned hybrid hydrogel system. C shows the bright field image of the channel after experiment. Control channel was a closed channel with no Rhodamine B flow.

The diffusive agarose microchannel was prepared as followed. Positive microchannel patterns were generated on silicon wafer with SU-8 2050 or 2150 photoresist. Microwave-heated 3 w/w% (in deionized water) agarose pregel was poured onto the wafer mold and cooled at room temperature for 30 minutes. The gel was then peeled and bonded onto hybrid gel (containing 0.2% Irgacure2959) substrate as described before to create microfluidic channels at the agarose-hybrid interface. The inlet and outlet region of the channels was punched with a puncher and tygon tubes were inserted for syringe-based flow generation. To verify microfluidic function and diffusion, 1mg/mL Rhodamine B solution was injected into the microfluidic channel at 5 uL/min and imaged with a fluorescence microscope.

When fluid (Rhodamine B) was injected, the 250um x 100um cross-section channel withstood the maximum pressure generated by the syringe pump's maximum flow rate (50 uL/sec, 2kPa). This was significantly higher than that obtained from a previously introduced agar-based microchannel system (0.22Pa).

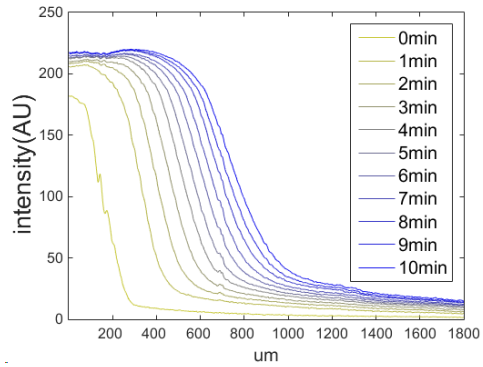

Figure 23. **Rhodamine B fluorescence intensity measured over time at the cross-section of the diffusive microfluidic agarose hydrogel system.**

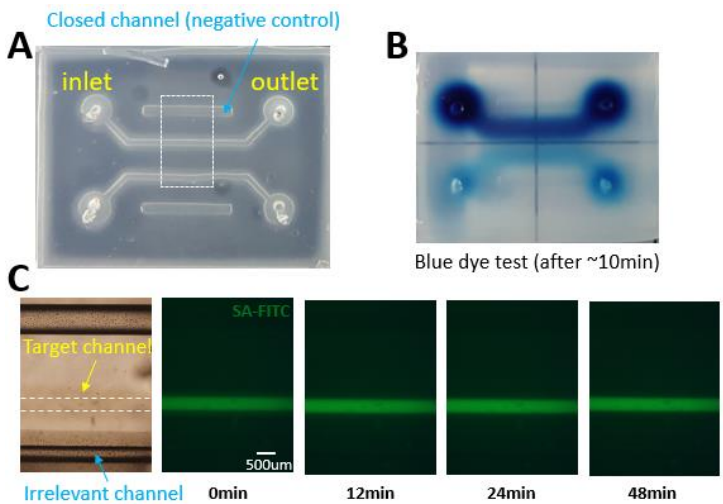

Figure 24. **The microfluidic chip design for the diffusive agarose hydrogel system.** A,B shows the bright field image. C shows target versus control channel flow experiment of FITC-conjugated streptavidin.

Naturally derived noncovalent hydrogels are usually too fragile to mimic biological organs. Via our bonding approach, our hybrid hydrogel, which was tough against bending stress, could be used to structurally support fragile noncovalent hydrogels. As a demonstration, we fabricated an intestine-like cylindric hydrogel structure. Even though it contained thin (1mm) noncovalent hydrogel, the structure withstood such significant bending stress. Noticably, agar-based tough hydrogel[30] ($\sigma_{fracture}$ =0.2-0.7Mpa, $\varepsilon_{fracture}$=180-260%) have similar mechanical property of small intestine[35] ($\sigma_{fracture}$=0.9Mpa, $\varepsilon_{fracture}$=140%). The intermediate raster scanning microchannel enabled diffusive fluid flow which could be useful in preimplant applications for cell-enriching nutrient/biomolecule supply.

Apart from `bendable` tough hydrogels, we also demonstrated bonding highly `stretchable` hydrogel[1] with noncovalent hydrogels using the same bonding method. We demonstrated an anti-fracture mechanism using the resulting agarose-tough hydrogel dual layer structure.

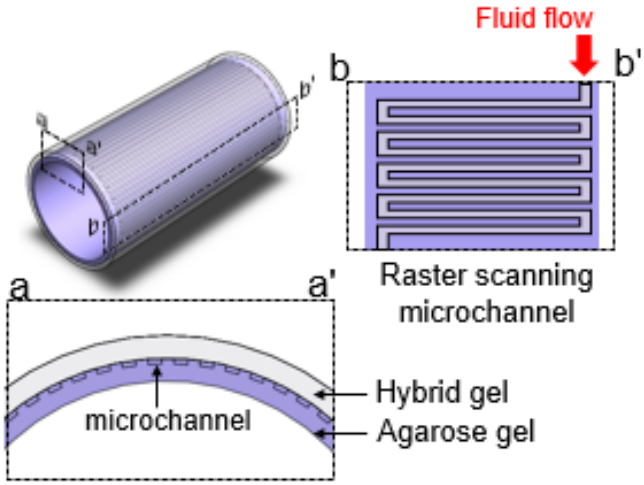

Figure 25. **Design of the hollow cylinder-shaped raster-scanning microfluidic chip.** The microchannel was patterned at the agarose hydrogel side

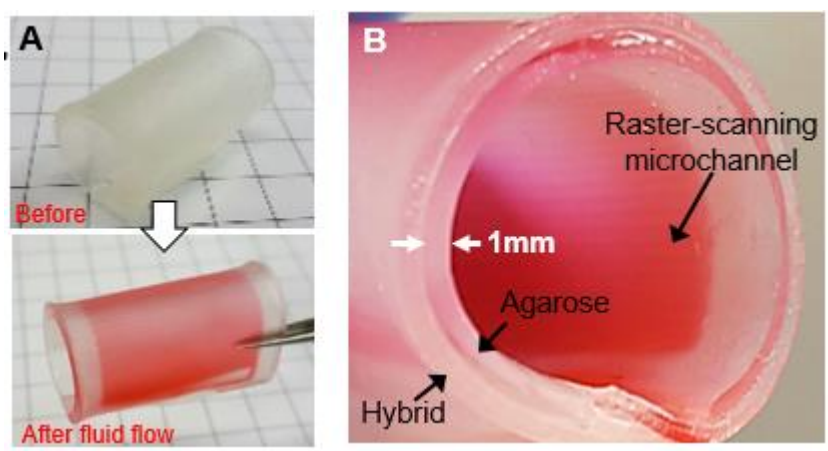

Figure 26. **Experiment result of red dye solution flow into the raster scanning microfluidic channel.**

When tensile strain was applied, the tough hydrogel compartment stretched while remaining attached to the already-fractured agarose fragments, thus preventing complete system fracture. We also demonstrated a gel healing mechanism but rather than obtaining both toughness and gel healing in one material[32], we juxtaposed tough hydrogel with healable hydrogel (low melting agarose, LMA) When tensile stress was applied, brittle LMA film shatterd into pieces but reassembled to its original orientation after stress relief. Therefore, heat-induced (1hr, 60°C) gel healing occured automatically without external fragment alignment. However, since our approach of gel healing requires a decent strain-free period it is not applicable to dynamic failure modes.

5.2 Electrophoretic oligonucleotide retrieval system

I also created an oligonucleotide-retrieving system by joining my agarose microfluidic structure with DNA electrophoresis.

Agarose based gel electrophoresis is widely used to separate DNA and RNA samples based on their molecular length. However, retrieving DNA/RNA with targeted length requires manual gel cutting and gel purification, which is rather labor intensive. In comparison, I was able to skip the gel cutting and purifying step by creating a ‘microfluidic DNA band retriever’ that can retrieve targeted DNA bands during electrophoresis.

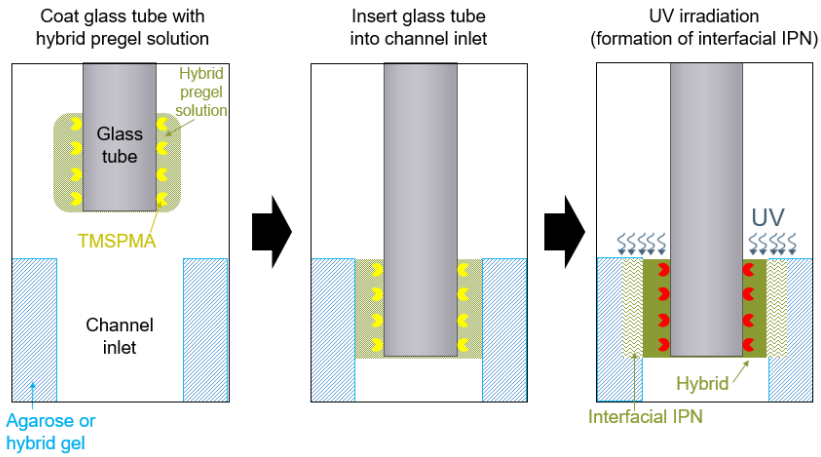

Figure 27. **Schematic description of how hybrid pregel solution can be used for generating a tightly sealed noncovalent hydrogel inlet to glass tube connection.**

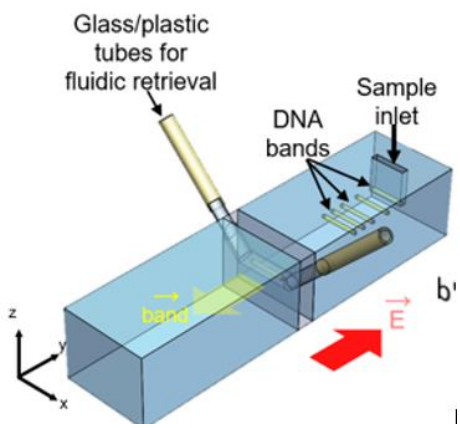

Figure 28. **Design of the electrophoretic oligonucleotide retriever.** The glass/plastic tubes for fluidic retrieval are inserted into the agarose/hybrid interface which is pre-patterned with a channel that goes through the path of oligonucleotide electrophoresis. As the sample is introduced into the sample inlet and electric field (red arrow) is introduced, the bands will move in the direction indicated in yellow

arrow. And when the target band passes through the channel , fluidic flow can be introduced to retrieve the band.

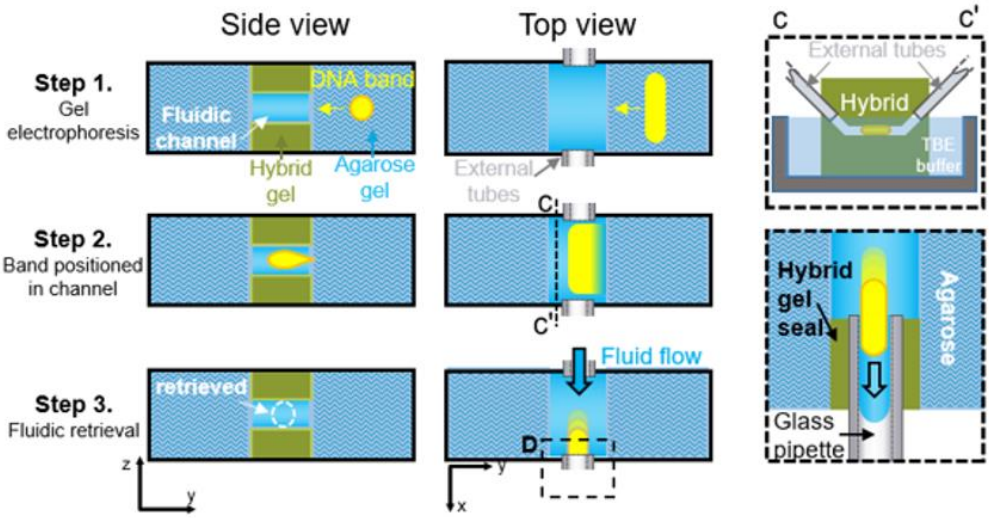

Figure 29. **Detailed step of electrophoretic oligonucleotide retrieval**

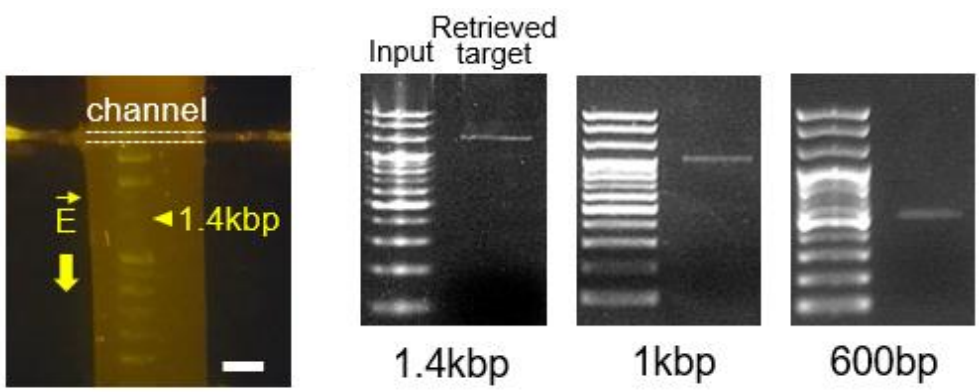

Figure 30. **Experiment result of electrophoretic double strand DNA (dsDNA) retrieval.** From left to right, the gel image after 1.4kbp retrieval, the retrieved 1.4kbp dsDNA, retrieved 1kbp dsDNA, and 600bp dsDNA sample.

I performed agarose:hybrid:agarose bonding to create a channel within the hybrid region. As electrophoresis continues, size-separated DNA or RNA bands pass through this channel. And the moment a DNA band with targeted length passes, the user can fluidically retrieve this band by withdrawing or infusing a syringe connected to the channel. The channel was designed to have a kinked structure so that only the DNA band retrieving region of the channel is submerged under the running buffer. This channel structure is critical since a simple straight line channel submerged in the running buffer creates miscellaneous electric field path along the microchannel and leads to unwanted diffusion of the DNA band.

I was able to retrieve a DNA band with targeted length within a sample containing DNA with various lengths. Although there were many reports of performing size-separating electrophoresis in microsystems, to our knowledge, this is the first attempt to retrieve an already size-separated DNA sample using microfluidics. Although inlets/outlets created by puncturing holes on hydrogels are, compared to stiff elastomers(e.g. PDMS), too fragile to tightly seal inserted tubes, our bonding method provided tight sealing between inserted glass tube and hydrogel channel inlet/outlet. This enabled robust target DNA suction without fluid leakage or pressure loss.

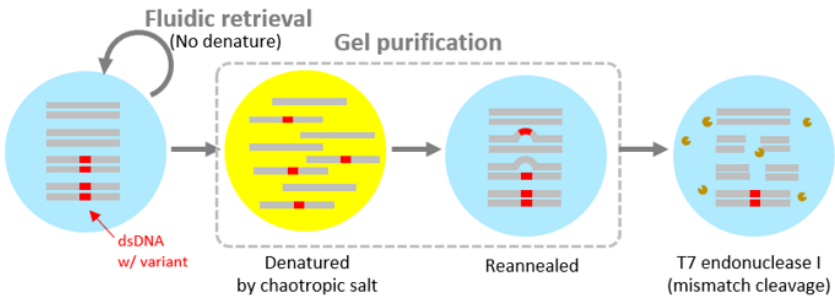

Figure 31. **Schematic description of the verification experiment of double strand DNA dehybridization and mismatch rehybridization occurred during gel purification process.** dsDNA with variant is dehybridized into ssDNA by chaotropic salt present in the gel melting solution and rehybridization by suspending in water leads to mismatch dsDNA (drawn as dsDNA with bulges). This mismatch can be broken into shorter dsDNA by T7 endonuclease I.

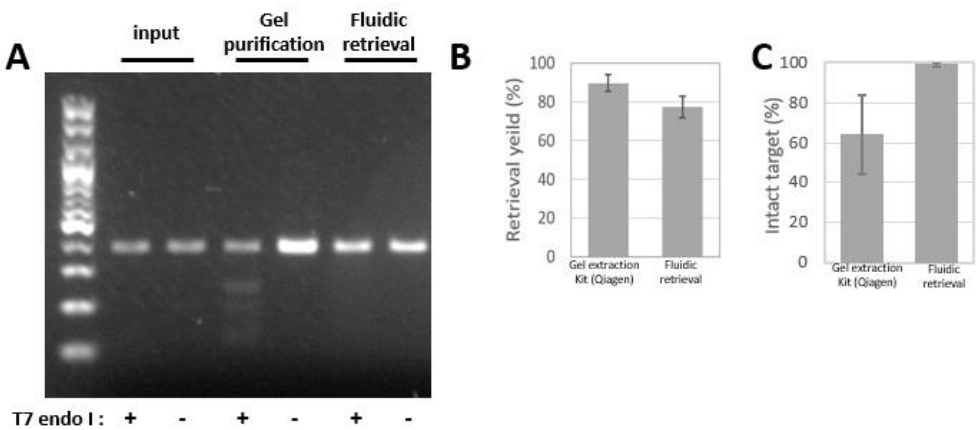

Figure 32. **Experiment result of T7 endonuclease I based mismatch dsDNA cleavage and yield comparison between conventional gel purification (Qiagen kit) and proposed fluidic retrieval.**

My device was capable of selectively retrieving target DNA bands (1.4kbp, 1kbp, 500bp) from DNA ladder samples. My method is more straitforward compared

to gel extraction method, which usually requires labor-intensive gel cutting, gel melting, sample purification, and strong chemicals (e.g. chaotropic salt) that damages oligonucleotide double helix. I performed T7 endonuclease I assay which showed that my fluidic retrieval method retrieves target samples without double strand denaturing.

5.3 Discussion

Micropatterned, cell-laden, noncovalent hydrogel scaffolds can be used for many applications including medium/drug-perfusion, chemotaxis, and extravasation simulations. Although these in vitro systems show similar biological function to the biological counterpart, they inevitably require good compatibility or coupling with external sensors and actuators.

Noncovalent hydrogels, as the name suggests, lack crosslinkable functional groups and thus require chemical modifications to be integrated on external microscopes, mechanical testers, electric circuits, and microfluidic devices. Diverging from previous reports where mechanical anchorage was the dominant approach for robust gel to solid attachment, we took advantage of the fact that most hydrogels are water permeable and can robustly bond with underlying solids by introducing an intermediate, chemically crosslinking hydrogel film. Noticeably, a single formula of hydrogel film can bond between various noncovalent hydrogels

and solids. Also the mechanism does not rely on extra adhesives or any reflow-generating sol-gel processes, thus allowing high-resolution microchannel formation or other micropatterned hydrogel-hydrogel interfaces.

In summary, I developed a versatile noncovalent gel-to-solid bonding method that utilizes a hydrogel-formed two-sided tape. My approach requires no mechanical anchorage, yet applicable to various noncovalent hydrogels and solids without design modification of the hydrogel tape. It also preserves interfacial micropatterns. With my approach, I increased stability and scalability of noncovalent hydrogel-containing structures as well as creating various novel functionalities. Therefore, I anticipate utilizing our approach to decipher further novel applications of noncovalent hydrogels in various bioengineering fields including in vitro assays, soft robotics, and tissue engineering.

Chapter 6

Single cell RNA sequencing application

The field of single cell analysis has been evolving rapidly over the past few years. One aspect has been the multiplexed analysis approach (analyzing more than one molecular type simultaneously from the same cell), the other has been increasing the throughput (number of cells analyzed per experiment).

There are many approaches to achieve these goals. In this chapter I introduce a novel approach that utilizes single cell electrophoresis as a way to retrieve oligonucleotide (DNA or RNA) from single cells onto barcoded microparticles. The novel part of this approach is that it has a potential to retrieve both DNA and RNA from the same single cell, with a high throughput capability, potentially tens of thousands of cells per run.

6.1 Introduction of the field and the proposed approach

The field of single cell analysis is evolving in two approaches. One is to increase multiplexity, the other is to increase throughput.

The former approach deals with the important quest in biology which is to understand how genotype influences phenotype. Masurements starting from a large population of cells or complex tissues, thus providing only an average measurement over the entire population. This obscures direct quantification of how genetic variability may affect the transcriptome at the single-cell level. Furthermore, as cell populations exposed to the same environment can also exhibit dramatic cell-to-cell variability in gene expression[5], the ability to understand the correlation between genotype and gene expression will require direct measurement of the transcriptome and the genome of the same cell. Current single-cell technologies are limited to quantification of either the transcriptome or the genome. In 2015, Alexander Van Oudenaarden developed a method to simultaneously quantify both the genome and transcriptome of the same cell. They used single cell isolation using mouth pipette. The mechanism of RNA DNA differentiation is based on statistics. The unique length-based identifiers found in the two cells can be used to count the original number of cDNA molecules this statistical method will not work for high-throughput multiplexed cell sequencing.

In another approach, high-throughput single cell analysis will allow i) to uncover cell lineage relationships, ii) supplant the coarse notion of marker-based cell

types, iii) allow discovery of functional states of individual cells, iv) analysis of rare cell types, and v) analysis of heterogeneous population. Therefore, high throughput single cell analysis has both big implication for basic biology and medicine.

In 2015, a number of papers from journals like *Science*, *Cell,* and *Nature Methods* showed that droplet-based, microwell-array based single cell preparation could lead to higher throughput (thousands of cells per run) of single cell RNA sequencing (Drop-seq, InDrop, Seq-Well, CytoSeq etc.). This led to a series of revolutionary studies that further increased the performance and throughput of single cell RNA sequencing, including the commericialized product (10x Genomics). The commercial product led to higher access of single cell RNA sequencing to biologists and clinicians who are not familiar with bioMEMS, microfluidics and optical setups. Eventually, numerous novel, high resolution biological discoveries are being made at many biological fields. Yet, there is an unappreciated shortcoming of this commercial product, which is the loss of sample quality over the duration of delivery from lab (hospital) to the location where the single cell RNA prep device is present. Although usually unofficial, there has been reports that RNA within live cells degrade rapidly (even within an hour) even in proper storage buffers. Consequently, the product user have no insurance that the single cell RNA preparation step is successful before using the product, at which step the user already have to pay for the service. This service alone (aside the NGS run needed) costs around 5,000 dollars

(in Korea). If unfortunately the run fails, the user has no choice but to do retrials of cell sample preparation and cell sample delivery with a more optimized protocol, until QC passes. This feedback could cost time, labor, and money.

6.2 Device design

Motivation of my project was the following.

If we emulsify cells in agarose gel (1.5%) and then lyse it, the extracted gDNA will be trapped inside the void of the lysed cell. (Richard Novak et al., Richard A Mathies group, Angew. Chemie., 2011, Single-cell multiplex gene detection and sequencing with microfluidically generated agarose emulsions).

Anticipation from the above fact is that if melt the agarose gel-trapped cell and perform gel electrophoresis, probably RNAs will come out ‘selectively’ and not DNAs. The trapped DNAs can be retrieved by re-melting(heating) agarose gel. Thus, we may separate RNA and DNA even within a single cell.

Next, for PCR reaction, the agarose emulsion (containing DNA ball & primer bead) was equilibrated with PCR mix, agitated for. The agarose droplets melt during the hot start phase of PCR and remain liquid throughout the amplification process, maximizing reagent and amplicon diffusion rates.

Predicted impacts of high-throughput single cell analysis	
Basic biology	- Uncover cell lineage relationships - Single-cell transcriptomics : Supplant the coarse notion of marker-based cell types - Single-cell epigenomics and proteomics: Discover the functional states of individual cells to be analyzed.
Medicine	- Analysis of rare cells ex) circulating tumor cell (CTC), cancer stem cell (CSC) - Analysis of heterogeneous population ex) tumor, peripheral blood cells

Table 1. Predicted impacts of high-throughput single cell analysis. Referred from Ehud Shapiro et al., Nat. Rev. Gen., 2013.

Based on this fact, I decided to develop a new single cell RNA preparation platform that makes this costly QC procedure cheaper, thus more affordable to general users.

The rough initial device design was like above. The cell can be assembled inside an agarose microwell array. The cells are then covered with melted agarose and let to solidify and fix the cells, Then another array containing DNA/RNA retrieving microparticles is assembled underneath the cell array, Then the entire construct is submerged in cell lysis and electrophoresis buffer. Immediately, the construct is placed under electric field to initiate electrophoresis. The RNA molecules will smear out of the cells and transfer to the microparticles. If one intends to retrieve the DNA as well, the DNA could be enzymatically sheared (using fragmentase or tagmentase) into smaller sizes. Then the DNA fragments can be retrieved by electric field onto the microparticles (if performed with properly designed probes).

If one intends to perform DNA FISH instead of DNA retrieval, one could simply submerge the RNA-retrieved cell array (now only having DNA within the cell array) can be submerged in FISH solution for FISH probe hybridization. The summarized advantage of this proposed method is as follows.

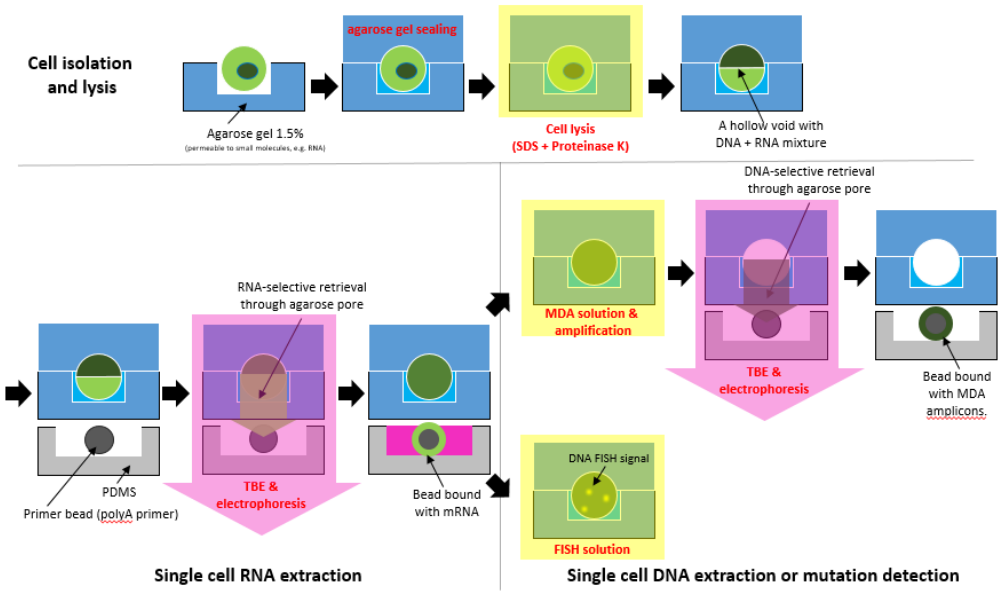

Figure 33. . **Initial design of sequential RNA, DNA retrieval from a single cell using agarose well and probe microparticle.** The DNA could be either imaged with FISH or amplified by MDA and retrieved to another microparticle by electrophoresis

Advantage of proposed method	
High throughput single cell analysis	- No averaging effect - Enables cell phenotype (morphology) identification before cytometry. - Sufficient sampling for statistical significance.
Genome-transcriptome paired analysis	- Direct correlation of gene state and gene expression - Allows to directly analyze genetic aberration (CNV, SNV) and gene expression perturbation. - No need for genome reconstruction from transcriptome analysis
Simple	- Only uses cheap agarose gel and electrophoresis - Easily accessible to basic biology lab.

Table 2. Advantages of proposed single cell DNA/RNA retrieval method.

6.2.1 Optimization of cell assembly protocol

The first step was to design the cell array. The material had to be sturdy enough to ensure microwell pattern, but also ensure hydrophilicity and porosity for electrophoresis. The easily approachable material was agarose, which is the conventional material for gel electrophoresis. To pattern the micro-wells, I utilized the conventional SU8 based MEMS fabrication. I first designed a mask for a microwell size of diameter 15-20um and total of approximately 10^6 wells per array.

The result showed that 1.5% agarose was capable of keeping the microwell patterns without distortion. The cells were then dispensed onto the agarose array. For this experiment, 1.3*10^6/mL of HL60 cells in their culture medium was directly dispensed on chip and precipitated for more than 10min. The remaining cells were then easily washable with PBS pipetting.

Then the cells were covered with agarose pregel solution.. Caution had to be made to ensure that majority of the cells remain within the wells and not detach from the wells. To assess this efficiency, the assembly efficiency was measured with MATLAB image processing. The cells were automatically recognized by analyzing circular features within the images. Cells that were assembled and remained after agarose fixation was tagged as blue. Cells that were disassembled after agarose cover was tagged as red, cells that were newly assembled were tagged as green, unassembled cells were tagged as yellow. The result showed that majority of the cells remained after agarose covering.

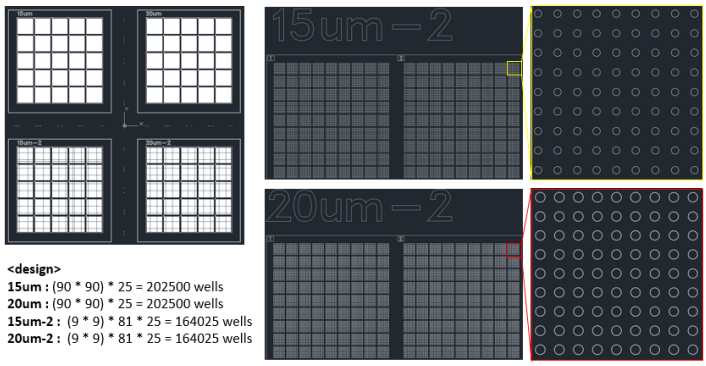

Figure 34. **Mask design used for agarose micro well design.** Either wells with diameter with 15um or 20um was designed. Using the mask I fabricated the negative pattern for microwell arrays (pillar arrays) using SU8 2015. From the pillar array, I poured on melted 1.5% agarose and let to solidify under ambient condition. The agarose well array was then peeled off and inspected under microscope.

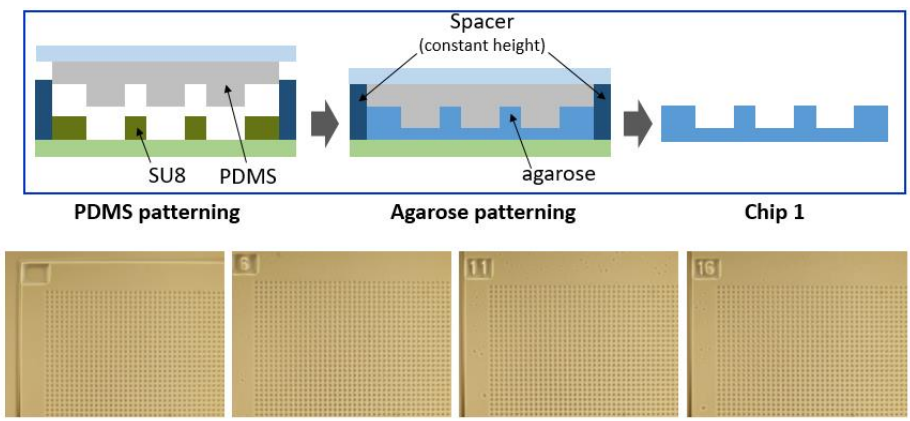

Figure 35. **Fabrication process of agarose micro-well chip and example result.** The SU8 pattern was molded into a PDMS mold. And the PDMS mold was then molded a second time with agarose hydrogel. The below four images are example of agarose wells.

.

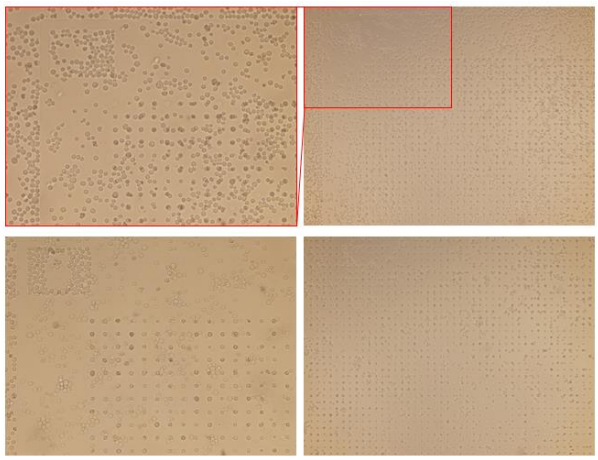

Figure 36. **Example images of cell dispensed agarose array.** The cells tended to assemble into the wells compared to non-well surfaces.

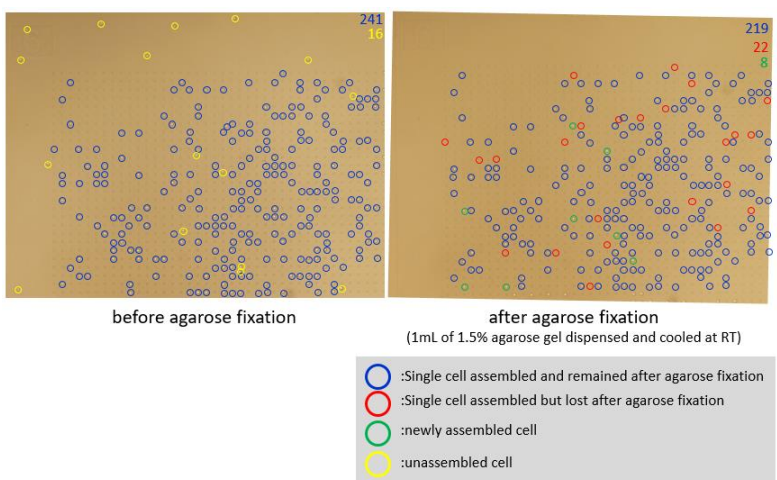

Figure 37. **Example result of cell assembly before and after washing.** The cells could be also stained with DNA or RNA staining materials such as Hoecsht, SYTORNAstain, and Pyronin Y. The results are shown below where around 80-90% of wells are assembled with single cells

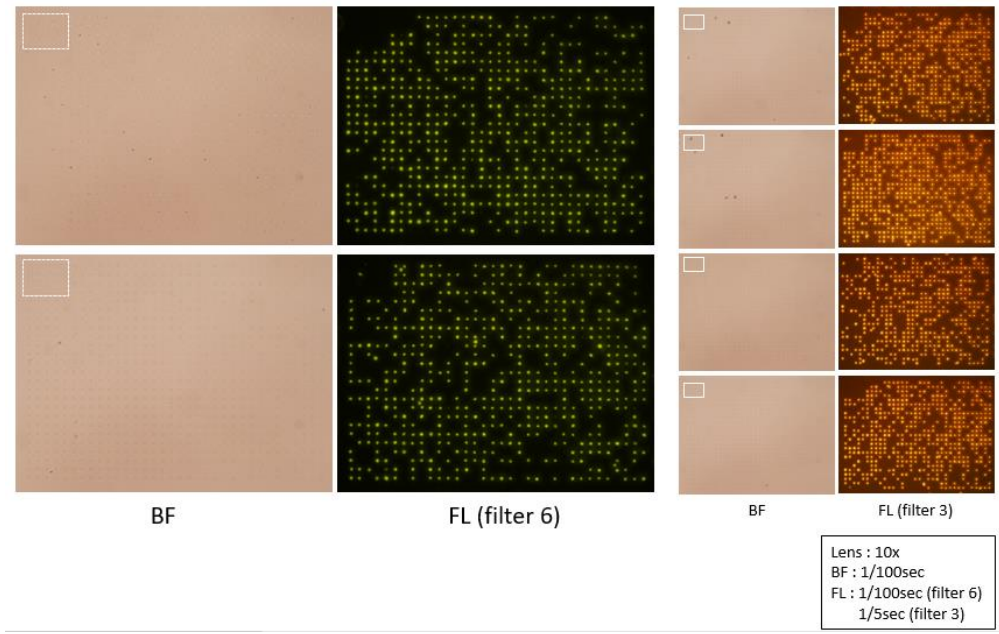

Figure 38. **Example result of cell assembly with fluorescently stained cells.**

6.2.2 Optimization of electrophoretic mRNA capture protocol

To see if I could retrieve RNA selectively and not DNA, I had to come up with a method to simultaneously stain both DNA and RNA within the cells. The method I used was to utilize Hoechst and Pyrinin Y.

For this I first harvested 10^6 cells (usually HL60 cells) in 1mL of cell medium and incubated with 5uL of Hoechst solution and let it incubate in the cell incubator chamber for 40minutes. After 40minutes I added 1uLof Pyrinin Y and incubated another 20 minutes in the cell incubation chamber. The cells were then washed with PBS. The cells were imaged under confocal microscope. The result showed that the cell nucleus was stained with Hoechst and the remaining cytosol and the Nucleolus (concentrated rRNA region) was stained with Pyrinin Y, as expected.

Then, using these stained cell, I performed a pilot electrophoresis test using the cell agarose array (covered with agarsose). The cell array electrophoresis performed with either no detergent or in the presence of detergent (Triton X).

For the Experiment group, 1.5% lw melting agarose (LMA) sealing gel with 0.5% Triton X detergent (10mM Tris buffer, 5mM DTT) was used. For the ctrl group, 1.5% LMA sealing gel without detergent in 10mM Tris buffer and 5mM DTT was used. After gel sealing both samples, they were kept in 4'C refrigerator for 20min for gel formation. The Experiment sample was treated with 400uL of "0.5% Triton in 10mM Tris, 5mM DTT solution" for 10minutes. And electrophoresis was performed with 230V for 20min vertical to the cell assembly plane.

The result showed that DNA (Hoechst stained) remained within the cell array where as RNA was extracted out of the cell array, leading to dimmer Pyronin Y fluorescence after electrophoresis. The reduction of Pyronin Y signal was bigger in the presence of detergent. This means that cell membrane lysis by Triton X enhances RNA extraction from the agarose array.

For efficient electrophoresis, I designed a specific chip holder. This holder contained two parts, each holding the cell array chip, the other holding the DNA/RNA capturing bead array chip. I specifically designed the holder to have the same dimension of common slide glasses. The center part of this chip contains the actual cell array and bead array chip. After the assembly of cell chip and bead array chip, electrophoresis can be performed with electric field orthogonal to the assembly planes.

This chip design was initially done for two reasons. First, the distance between the cell and the bead that is intended to retrieve the cell's DNA/RNA had to be minimized. For this, the way to reduce this distance was to use the LMA agarose cover of the cell/bead array as the path of electrophoresis, which is estimated to be 100um. Second, the chip had to be thin to ensure optical imaging of the cell array plane and the bead array plane even after chip assembly. This is critical so that proper cell and bead array aligning.

Figure 39. **Example Confocal image of Hoecsht and Pyronin Y stained cells.**

•

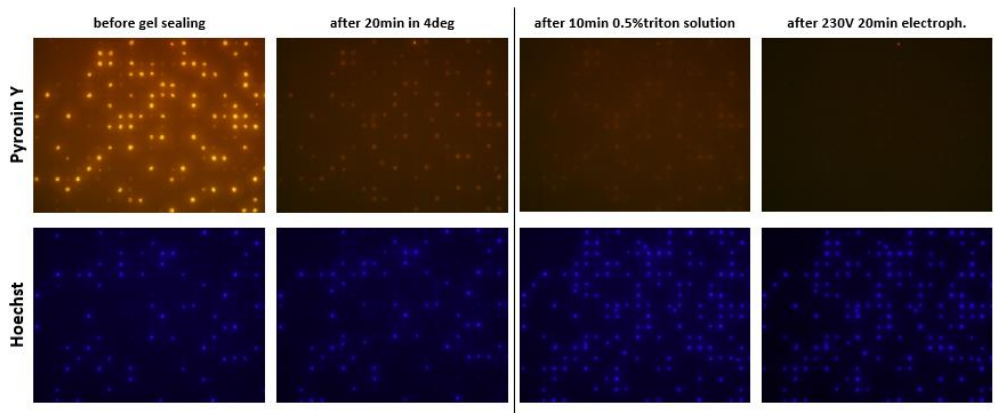

Figure 40. **Electrophoretic RNA selective retrieval demonstration using Hoechst/Pyronin Y stained cells.**

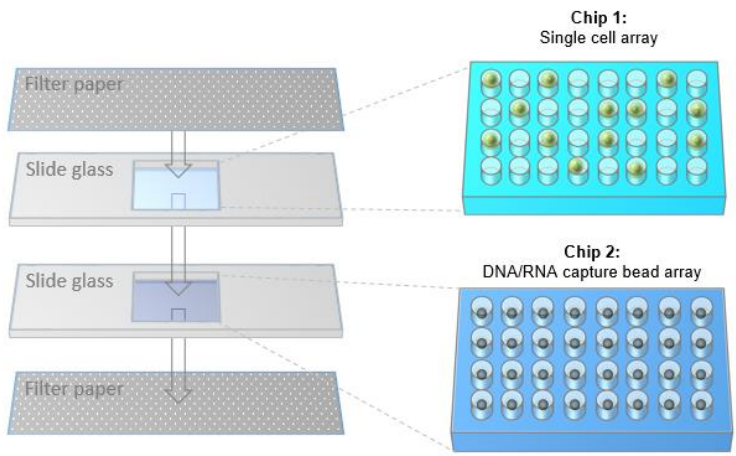

Figure 41. **Schematic example of cell array and bead array assembly.**

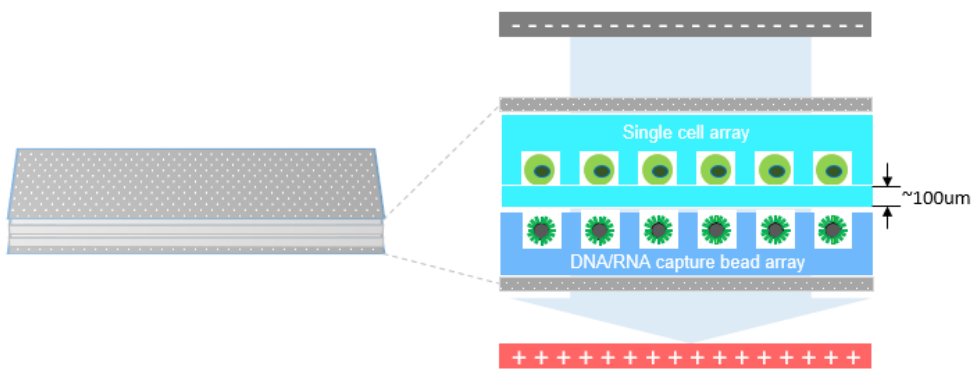

Figure 42. **Schematic example of electrophoresis from the assembled cell/bead array.**

Advantages of the proposed device was as follows. First, it is easy to fabricate chip1 and chip2 with no height variation among replicates and perfect height flatness can be realized. Second, thin chips (~1mm thickness) can be handled without buckling or tearing. Third, they are easy to align and assemble chip1 and chip2. Finally, it is easy to perform electrophoresis since no detaching between the chips and filter paper stops the gels from falling apart from the slide glass.

6.2.3 Crosslinking mRNA capturing probe onto magnetic microparticles

The mRNA that is extracted from the cells have to be captured onto the microparticles. For the actual experiment, the probes have to be synthesized on the bead. This is critical because one needs cell barcode, which in turn needs split pooling. However, at this point I first had to verify that mRNA can indeed be captured on the microparticles and amplified by RT-PCR. For this I only needed the primer region (TSO) and the polyT region on the beads. To make this, I needed carboxyl magnetic microparticles and 5'-amine modified ssDNA probes pre-synthesized by custom primer ordering. The chemical crosslinking was performed with a conventional EDS based carboxyl-amine crosslinking.

For this. I ordered carboxyl polystyrene microparticles (diameter of 20um) from Spherotech. The beads were washed with MES buffer three times. Then the

beads were mixed in DNA probe (5'-amine-TSO-T30) and EDC (approximately 0.0033mg/uL). The mixture was incubated in room temperature mixter with 1500rpm vortexing for 1 hour. The beads were then washed with 1% SDS in TE once, TE buffer twice and stored in TE buffer at 4℃.

Then I first verified that the probes were assembled onto the beads by incubainting with Cy5-dT probe hybridization. For this the Oligo-MMP (or bare MMP) was mixed with Cy5-dT and incubated at 25℃ for 30min incubation in the dark while vortexed every 5min. The beads were then wash with TE buffer 2 times. The beads were imaged with fluorescence microscope.

6.2.4 Optimizing RT-PCR protocol for single cell or small number of cells using mouth pipetting

Next, I had to adjust the previously reported reverse transcription and PCR reaction (RT-PCR) to my proposed system. To do this, I first replicated the classical single cell RT-PCR protocol. To perform such classical single cell RT-PCR, I performed glass mouth pipette based single cell retrieval.

I prepared such glass microcapillaries using glass capillaries with 10-20uL volume capacity. The glass capillaries were extended with the glass heating and pulling device. Then the tip of the narrowest part was delicately broken to have an opening diameter of 10-20um. The capillary was then assembled to a custom mouth

pipette mounting device. In detail, 20uL glass micropipettes were purchased from Hyunil Lab-mate “e-shop” (cat no. HSU-2920110). Heat-pulling was performed with the standard 2-step pulling protocol. Pipette tips were manually grinded by simply scraping against a kimwipe paper. Final tip inner diameter was around 10~20um. The tail of the glass capillary was connected to a tube, connected to a syringe. The syringe was used to perform air suction. This device was assembled to a bench top microscope. HL60 cells for single cell retrieval was dispensed on a glass slide was then imaged with the microscope while the glass capillary was used to target single cell. Syringe suction ended up with retrieving the target single cell. The retrieved cells and be ejected by simply ejecting the syringe.

From the retrieved cells, I performed RT-PCR using the following protocol. For one sample, I pipeeted 10 cells into a PCR tube cap that contains 3.75uL of cell lysis solution (nuclease free water with and RNAse inhibitor and dNTP mix and Triton X). As soon as the cell was ejected into the cell lysis solution, the cells melted right away, releasing the RNA content. To the RNA, 1 μL of 10 μM UMI_SMARTdT primer was added and sealed with a PCR tube. The tube was then heated to 72°C for 3minutes or 65°C for 5minutes. Then the tube was immediately put onto ice for fast temperature drop. This ensures that the secondary structure of the mRNA are not recovered and efficiently hybridized to the poly T probe. Then the RNA was mixed with RT buffer, RT enzyme (Maxima or Superscript IV), and template switch oligo

(TSO). The mix was incubated at 42°C for 90 minutes, followed by heat inactivation for 5 min at 85°C. The sample was then mixed with KAPA polymerase mastermix and PCR primers. The entire mix was then went under PCR cycles. The samples were purified with 0.6x AMPure XP beads according to the manufacturer's instructions, and eluted in 10 μL H2O. The control samples were pure RNA inputs instead of the 10 cell, no reverse transcriptase control, no input RNA control, and no PCR reaction control. The RT-PCR samples were injected into 1.5% agarose and gel electrophoresis was performed at 180V for 20minutes. RT bands appeared from 10 cell lysate RT-PCR experiments although each PCR sample contained only 40% of the total cDNA from 10 cells. However, the overall length distribution of the RT-PCR bands from 10 cell lysates were shorter than RT-PCR bands from pure RNA. This could indicate ①inefficient RT reaction due to cell lysate ②insufficient cell lysis and loss of long mRNAs ③ mRNA degradation (although unlikely because we added Superase In) ④ mRNA secondary structure (unlikely, because we have a 72deg 3min denaturation step during cell lysis and polyT-primer hybridization)⑤ RT inhibition due to mRNA-bound proteins. The RT-PCR band from pure RNA didn't alter although the composition of RNA hybridization of RT reaction mix changed a little (additional 0.2% Triton X-100 and Superase In). Then, I decided to perform on-bead RT-PCR using the oligo crosslinked MMPs synthesized previously.

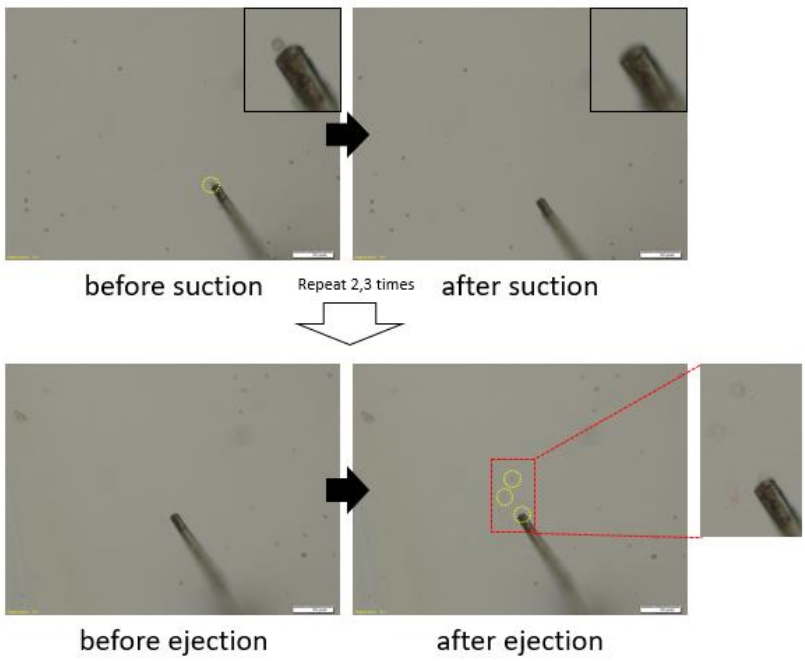

Figure 43. **Example result of micropipette based cell retrieval and ejection.**

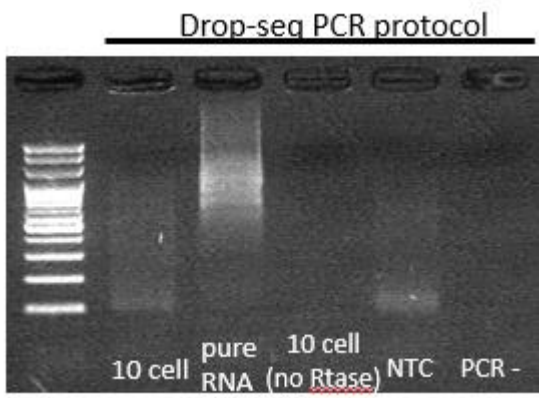

Figure 44. **RT-PCR result from small number of cells. 10 cell sample was the RT-PCR result from 10 mouth-pipette retrieved cells.** Pure RNA sample was the RT-PCR result from 300pg of purified RNA. NTC: no template control. PCR- : same condition with pure RNA sample but with no PCR.

For this, 5AMC6-TSO-N12-T30VN and 18.5um carboxyl MMP was used to prepare the mRNA-capturing probe with the previously explained amine-carboxyl crosslinking protocol. Then 5uL of 16ng/uL total RNA was incubated with approximately 1500 probe MMPs (5uL of stock solution) in 40uL Fodor lysis solution (10x TE, 0.5% SDS, 500mM LiCl) and incubated at 25°C for approximately 1hour at 1500rpm. This ensures the mRNA are hybridized onto the probe MMPs. The resultant was washed once with TE/SDS (1x TE buffer mixed with 0.1-0.5% SDS), twice with TE/TW (1x TE mixed with 0.01-0.1% Tween 20) and once with RT buffer.

For the RT reaction I used; 2uL RT buffer, 0.4uL dNTP, 0.5uL Superase In, 0.625uL TSO, 2uL 20% Ficoll, 4.5uL NFW, 0.5uL maxima Rtase. RT reaction was performed by the following cycle; 25°C 30min, 42°C 90min, 50°C 2min, 42°C 2min, 4°C forever. The resultant was washed once with TE/SDS, twice with TE/TW and once with NFW. For each washing step, solution volume was 100uL. The beads were mixed with 25uL KAPA HiFi 2X, 4uL TSO-PCR primer (10uM solution) and PCR was performed for 14 cycles. The result showed proper cDNA length distribution of 0.5-3kbp. Therefore, the on-bead RT-PCR was successful and the actual experiment can be performed as expected.

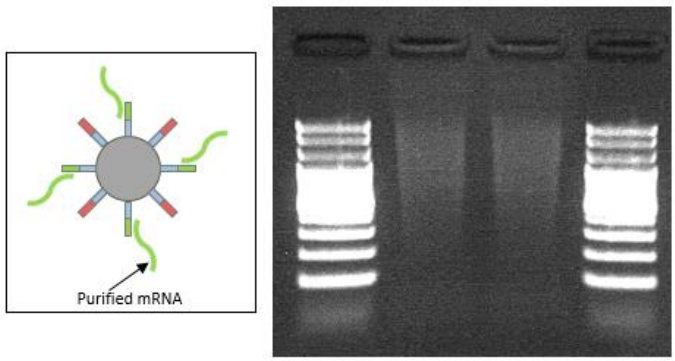

Figure 45. **RT-PCR result from on-bead mRNA capture and RT-PCR.**

6.2.5 Critical limitation of the approach

There were a number of problems that were unsolvable. First, the assembly part, assembling the cell array and the bead array was unrealistically difficult. This was because the agarose array itself was too fragile to enable cell to bead exact assembling. Also, even after aligning the cell-bead array, they didn't remain aligned because slipping occurred between the cell and bead array. Also, the array being fragile led to unwanted distortions within the array, making it almost impossible to make a perfect alignment. Second, when cell lysis and electrophoresis was performed, the RNA within the cells didn't directly transfer to the bead. It rather diffused throughout the whole cell array, leading to cross contamination between cells. So unlike DNA, mRNA diffused rapidly within the agarose chip.

Chapter 7

Single cell RNA sequencing with microcapillary array

Glass microcapillary array turned out to be an optimal substrate for parallel single cell electrophoresis. Since it is made of glass, it is inherently resistant against cross contamination of extracted RNA. However, there were unverified obstacles such as assembling the cells and beads to the either end of the capillary. In this section I discuss the process I went under for getting capillary agarose filling conditions for optimum capillary well formation, cell assembly, bead assembly, and performing electrophoretic RNA retrieval.

7.1 Single cell electrophoresis protocol optimization

7.1.1 Optimization of barcoded mRNA-capturing microparticle synthesis

The mRNA-capturing probes and the particle needed for this experiment has to suffice the following conditions.

First, it has to contain a primer region (R1P or TSO), cell barcode, unique molecular identifier (UMI), and a poly T region.

Second, the probe has to be attached to a magnetic microparticle (MMP) with uniform diameter equal to the capillary diameter, which is 20um. Also, the probe's 5' end has to be attached to the MMP so that the 3' end of the mRNA, which is the poly A tail, hybridizes with the poly T region of the probe.

Third, the MMP has to withstand the highly nonpolar, oxidizing, pH-varying conditions of the oligosynthesis procedure.

Finally, the cell barcode of the probes have to be uniform within one particle but have maximum discrepancy with cell barcodes from other particles.

To cover all these conditions, I decided to perform on-bead oligosynthesis using reverse phosphoryl amidites. Unlike conventional amidite based oligosynthesis, the synthesis occurs in the 5' to 3' direction. Also, for the cell barcode synthesis part, split pooling had to be performed.

Split-pooling of oligosynthesis is a technique that enables particle-specific

barcoding using a series of i) splitting the particle pool into 4 samples, ii) performing unique single amidite synthesis for each sample, and iii) then pooling the samples again. By repeating M cycles of this split-pooling cycle, one could produce M-mers of cell barcodes.

For the UMI synthesis, we mixed four amidites with equimolar concentration. Simply mixing equal volume of the amidites would lead to non-equimolar mix since each amidite has different molecular weight and each amidite solution contains only fixed gram per liter concentration.

In respect of the MMP used, simply using polystyrene magnetic micro-particles resulted in complete melting of the particles during the oligosynthesis cycle. This was due to the oligosynthesis cycle containing highly nonpolar solvents which polystyrene is vulnerable against. After a number of trial-and-error, I discovered that a highly cross-linked polystyrene (approximately 60:40 = DVB:PS, DVB is a polystyrene crosslinking material) can withstand the harsh chemical conditions. So for the actual oligosynthesis, this highly crosslinked paramagnetic polystyrene micro-particle was used.. The para-magnetism was needed for proper bead assembly onto the micro-capillary array and washing steps after RT-PCR.

To explain from start to finish of the mRNA-capturing oligosynthesis, I first washed the MMPs with Acetonotrile (ACN) twice and position on top of an oligosynthesis column. The column was then mounted on a Mermade machine. I first

synthesized the primer region of the mRNA-capturing probe. Five Ts were positioned at first which works as a flexible spacer. T was chosen since Thymidine is known to produce the less stacking effect, thus most flexible. The primer region was 3' part of the Truseq Read 1 primer or the TSO primer. Then the cell barcode was synthesized using 12 cycles of split pooling. Then 10 cycles of random amidite synthesis was performed to make the UMI region. And finally, 30 Ts were synthesized. The beads were then retrieved from the column and washed twice with 100% EtOH, twice with pure water. Then the beads were submerged in 30% Ammonium hydroxide in a glass bottle. The bottle was sealed with paraffin film and was placed in a 80°C oven for 5 hours. This was the deprotection reaction needed to remove the protection groups covering the bases.

To verify that the oligosynthesis was performed properly, I performed bulk RT-PCR reaction with purified total RNA and these oligosynthesized beads. For this, I first purified approximately 100 to 1000 ng of total RNA (which of 1-5% are known to be mRNA) using Qiagen RNA purification kit. The purified RNA was mixed with the oligo MMP in a high-salt condition (0.2-0.5M LiCl, 0.2-0.5% SDS, 10x TE) and vortexed at room temperature for 30-60 minutes at 1100rpm. The beads were then washed with nuclease free water several times. Then the beads were mixed with reverse transcription mix (containing dNTP, RT buffer, Maxima Reverse transcriptase, RNase inhibitor, and TSO). Reverse transcription was conducted at 42°

C for 90 minutes. Then Exonuclease I (Exo I) was added to the mix and incubated at 37°C for 30minutes to remove all single strand probes remaining. This step is necessary, because if not removed, the single strand probes lead to cross reaction with barcoded cDNAs leading to obscurely barcoded cDNA production and other nonspecific amplicons. Then the beads were washed with 1x TE buffer a few times and mixed with PCR reaction mix (containing KAPA high-fidelity polymerase and buffer, and PCR primers) and went under PCR cycles (10-15 cycles).

The length distribution of the resulting cDNA amplicons were imaged with agarose gel electrophoresis. Proper cDNA length distribution is a smear between 500bp - 3kbp. The result showed a smear between 500bp to approximately 3kbp as expected.

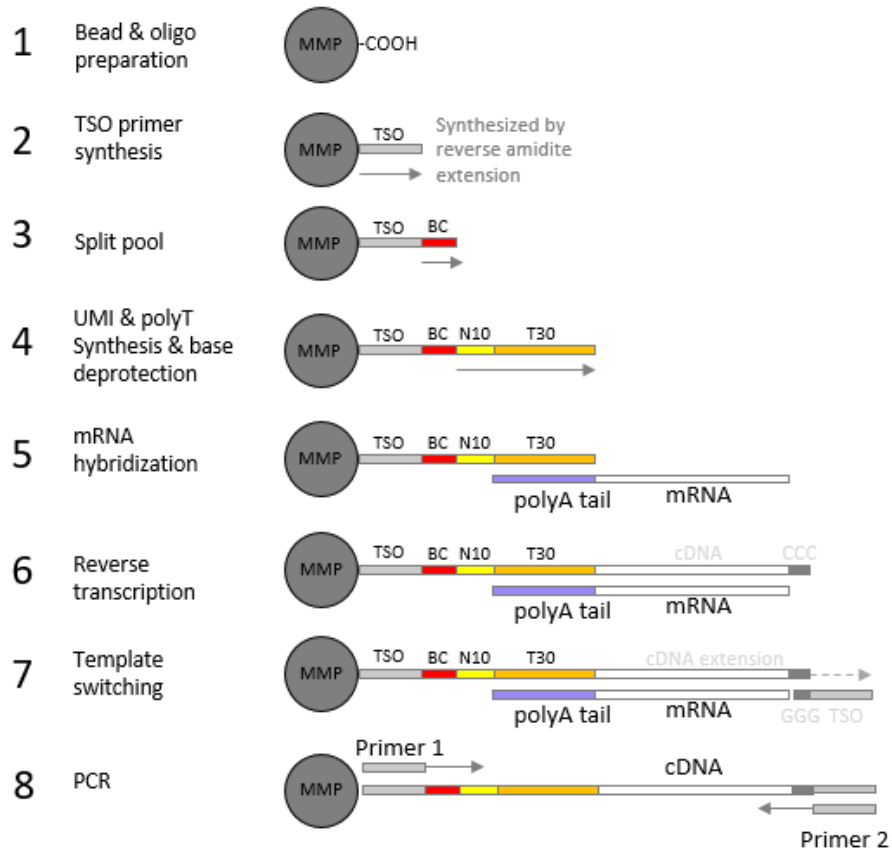

Figure 46. **Procedure of synthesizing RNA capturing and barcoding magnetic microparticle (MMP) and RT-PCR of captured mRNA.** The MMP contains carboxyl groups on the surface on which reverse amidite synthesis can initiate. The PCR primer (TSO) is synthesized first. Then cell barcodes are synthesized by a series of split pooling (usually 12 cycles). Then 10 cycles of random nucleotide synthesis creates unique molecular identifier (UMI) and 30 thymine is synthesized (step 1-4). After ammonium hydroxide based deprotection, the beads are ready for mRNA capturing. mRNA is captured by its poly A tail, then reverse transcriptase synthesizes cDNA and a triple C overhang. The template switch oligo (TSOrGrG+G) hybridizes to this overhang and template switching occurs. The TSO on both side is now used for PCR.

7.1.2 Optimization of cell assembly and bead assembly

Next, to make the actual micro capillary array I had to come up with a protocol that i) fill the empty glass capillaries with agarose, ii) produce capillary wells at both side ending of each capillary with relatively uniform depth, iii) assemble oligo beads at one side of the agarose-filled capillary array with acceptable filling rate, iv) assemble cells at the other side of the capillary array with acceptable single cell assembly rate (having acceptably low doublet, triplet cell assembled wells), and v) covering the beads and cells to prevent from detaching.

For the agarose filling step, I used low melting agarose that remains as liquid at body temperature. Therefore, the capillary array can be submerged in the agarose liquid for sufficient time for all the air bubbles within the capillary to escape and make full agarose filling. Then the capillary was recovered from the agarose liquid and let to solidify under room temperature. However, when simply filling the capillaries with LMA, the agarose gel within the capillaries tended to slip out due to lack of strong surface adhesion between agarose and the glass capillary. Fortunately, the hydrogel-to-solid bonding technique became handy at this point. I speculated that by adding a little AAm monomer within the agarose liquid while the glass capillary being coated with TMSPMA beforehand could lead to stronger agarose to capillary bonding, thus preventing slippage.

For the oligo bead assembly part, the task was simple. By simply dispensing

the oligo MMPs onto the agarose-filled capillary array and scraping with cell scraper led to sufficient bead assembly rate. When a strong magnet was placed on the other side of the array, the assembly efficiency increased further. On average, the bead assembly rate (number of capillary wells assembled with bead) was around 70-90%.

Next, for the cell assembly part, simple cell scraping was not effective. It seemed that the cells had lower density compared to beads and therefore lower tendency of sedimentation into the capillary wells. Also, cell scraping led to severe cell bursting and shearing. And simple dispensing of the cells ended up with the majority of the cells suspended within the agarose cover layer, not positioning at the capillary well plane.

To overcome this, I utilized the fact that this capillary wells were an open well that allows water flow towards the bottom of the capillary well. When I placed tissue papers for water retention on every corner of the capillary array and dispense cell suspension solution, a capillary flow occurred downwards. This in turn made automatic cell assembly. When compared to conventional microwell single cell assembly methods, my apporoach has superior cell assembly rate (number of cells assembled compared to input cell) because most of the cells are automatically assembled into the capillary wells and not lost due to any washing step or non-alignment. In other words, most of the input cells are assembled into the capillary wells.

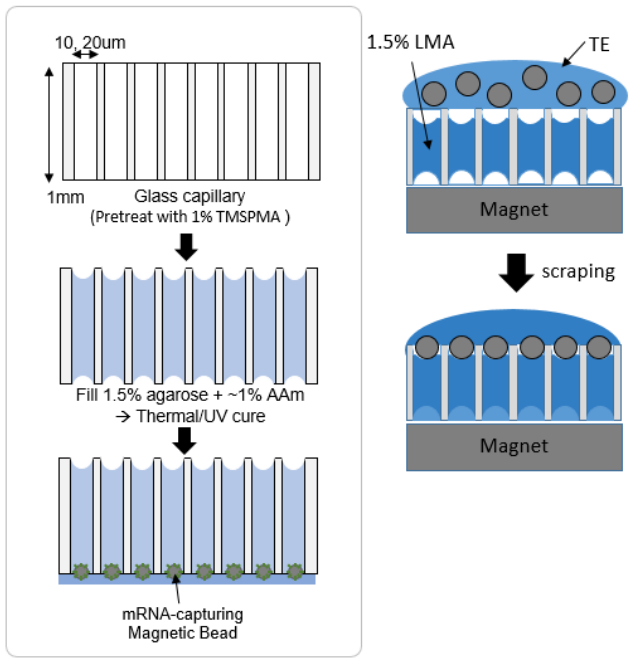

Figure 47. **Method of preparing agarose-filled, bead assembled, microcapillary array.** The glass microcapillary is first submerged in 1% TMSPMA solution for TMSPMA coating. Then the capillary is submerged in 1.5% low melting agarose (LMA) solution at 37°C overnight for filling the capillaries. Then the chip is removed from the solution and gelation occurs at room temperature. In the capillary wells, the beads are assembled by cell scraping while a strong magnet is placed on the opposite side.

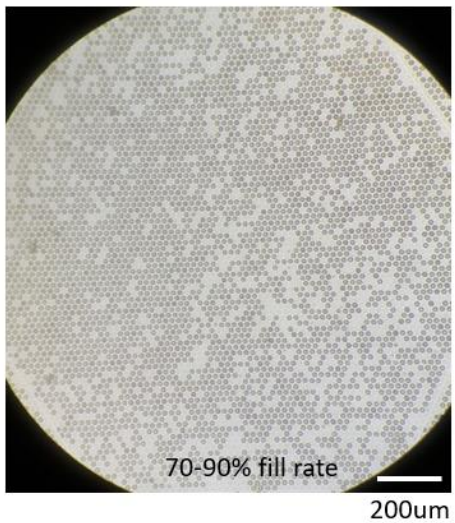

Figure 48. **Example image of bead assembled.** The 18.9um diameter MMPs were assembled into the 20um diameter capillary wells with 70-90% filling rate.

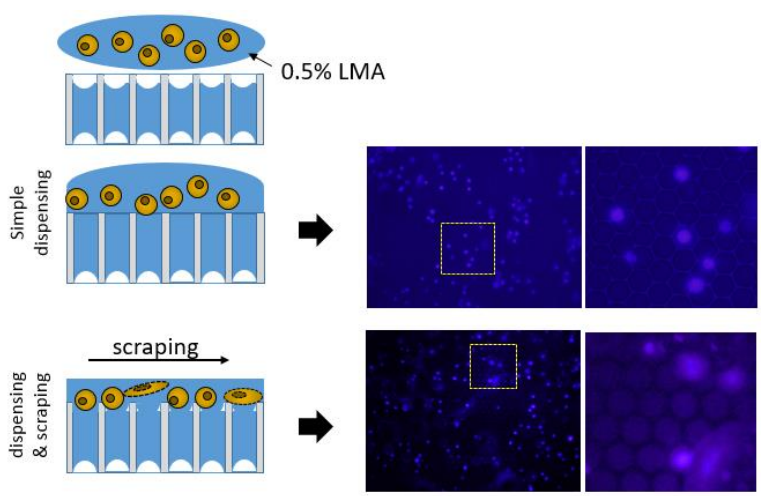

Figure 49. **Trials of two cell assembly methods.** Simple dispensing (upper row) ended up with most of the cells not aligning with the capillary wells. Cell scraping after cell dispensing (low row) ended up with damaged cells due to the high viscosity of agarose compared to water.

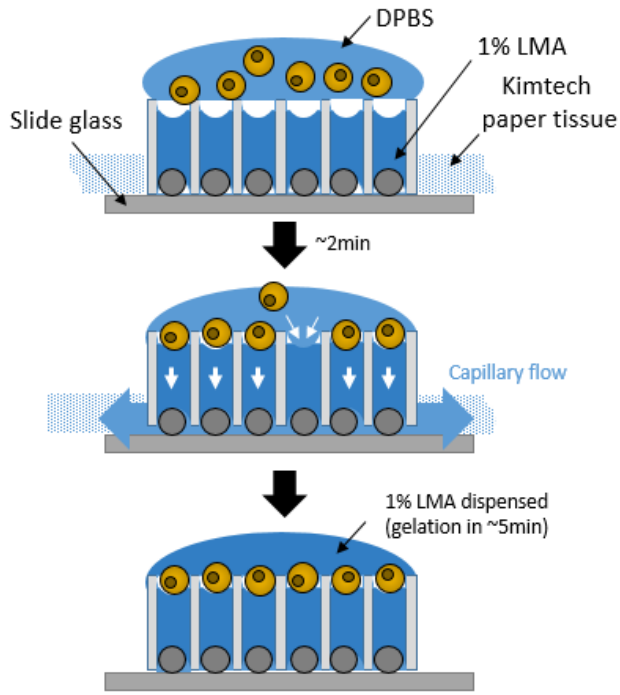

Figure 50. **Third method of cell assembly using capillary flow based cell suction.** Since the capillaries are open on both side, the cell medium (in this case DPBS) can penetrate into the capillary wells and exit through the bottom side of the capillaries. The exited medium can be soaked by paper tissues by capillary flow. This capillary flow induces the cell assembling effect. After the cells are assembled and the cell medium is mostly removed, a 1% LMA solution is dispensed and let for gelation which leads to cell sealing and physical fixation.

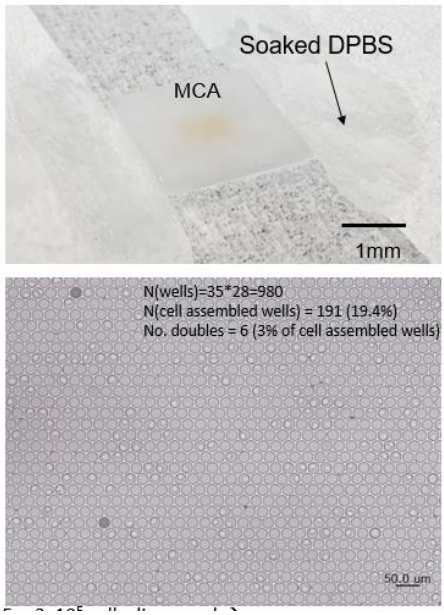

Figure 51. Experiment result of third cell assembly method using capillary suction.

This could lead to advantages in analyzing rare cell samples. In my case, when introducing 1-2 x 10^5 cells as input, approximately 10-20% of the capillary wells were assembled with cells, of which 95-97% were single cell assembled. The remaining 3-5% were usually doublet assembled wells. This is in good accordance with the fact that this chip has approximately 0.8-1 million wells and 1-2 x 10^5 cells is about 10-20% of the number of capillaries. To measure the cell assembly efficiency, I used HEK293T cells prestained with Hoechst, at 37°C for 40minutes, washed with DPBS and suspended in DPBS.

7.1.3 Optimization of electrophoretic mRNA capture protocol

For the actual electrophoresis to be performed, I had to make a custom holder for the capillary array. First, since most electrophoresis bath are usually horizontal, the capillary array has to be vertically fixed. Second, the buffer for electrophoresis had to be modified so that it contain proper detergent for cell lysis and high salt concentration for efficient mRNA to probe hybridization. However, high salt concentration leads to high current flow, thus voltage drop. So excessive salt could lead to insufficient electric field for electrophoresis itself. I had to adjust the salt concentration to an appropriate level so that it produces sufficient electrophoretic mobility of mRNA while not too low so that it has no positive effect on mRNA hybridization. Also, the electric field itself had to be adjusted so that the electrophoretic mobility is not too high that mRNA just pass by the oligo MMP without hybridization. Also, the high salt concentration of salt leads to heating of the buffer. High temperature is detrimental to mRNA to probe hybridization. So, to minimize temperature increase, I minimized the lysis/hybridization/running buffer volume (approximately 3mL), by creating an agarose based chamber. This chamber was prebuilt before electrophoresis by designing a removable mold within the capillary array holder. 5% agarose hydrogel solution was poured into the agarose chamber mold and let to solidify. After gelation, the spacers were removed. Then the capillary array can be inserted in the middle and the inner chamber can be filled with the modified buffer. The outside of the holder was filled with conventional

electrophoresis buffer (0.5x TBE).

For the holder design, I designed with SolidWorks and fabricated with Acrylic plates. The initial design was a single body holder with 4 blockers. However, due to practicality issues, I modified into 3 body holder and 4 blocker design. The 3 body parts were glued together with acryl glue.

After heuristic analysis, I found out that at 1V/cm electric field, and buffer condition of 275mM LiCl, 10x TE, 0.2% SDS, dsDNA, regardless of dsDNA length between 100bp to 3kbp, showed approximately 1mm/10min velocity across a 1.5% agarose hydrogel. I assumed that RNA electrophoresis velocity would be in the similar range.

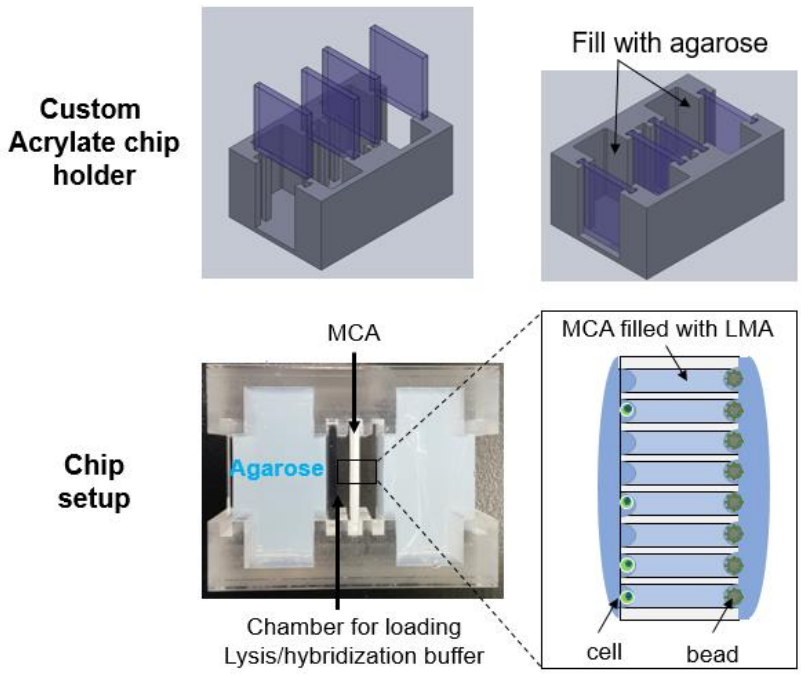

Figure 52. **A custom acrylic MCA holder.** The four acrylic blockers are assembled. for creating the agarose blockers. The agarose filling chambers are filled with approximately 5% agarose solution and let for gelation. The blockers are removed and the MCA assembled with both cell and MMPs are assembled.

7.2 Single cell RNA retrieval demonstration

7.2.1 Single cell mRNA retrieval test

For the demonstration of single cell mRNA retrieval, I used one of either HL60, HEK293T, NIH3T3L1, or EZ7 cell. HL60 and EZ7 are tumor cells. HEK293T is a human embryonic cell line. NIH3T3L1 is a mouse fibroblast cell line. All cell lines were cultured with the recommended medium and condition by ATCC. 1% Penicillin and Streptomycin were also added to prevent bacterial growth.

For cell staining, I used Hoechst as before. 1mL of 10^6 cells were added with 1uL of Hoechst 33343 and incubated in the cell culture chamber for 40 minutes. After that, cells were washed with DPBS. To stain the mRNA molecules Pyronin Y was not a proper choice since it may prevent mRNA hybridization to the DNA probes. Also the strong detergent (SDS) present in the running buffer could prevent proper staining.

So instead of using Pyronin Y, I decided to use a fluorescent polyT probe; a 30 T single strand DNA that has a Cy3 or Cy5 fluorescent tag at the 5' end. The way this probe tags mRNA is as follows. First, as I perform electrophoresis, mRNA will be extracted from the cells. Then, the mRNA molecules will bind to the polyT region of the oligo bead by their poly A tail. After sufficient electrophoresis, I then add the fluorescent polyT probe to the running buffer. The fluorescent probes would then bind to the remaining single stranded polyA tail region of the mRNA molecules. Sufficient electrophoresis would wash out any remaining fluorescent probes. This

way, only the oligo-beads that have retrieved mRNA molecules on it would be fluorescent. Also, the fluorescence intensity would give qualitative measures of how many mRNA molecules are bound to the oligo bead.

For the actual experiment, I used mostly HL60 and EZ7 cells. First, filled the glass microcapillary array with 1.5% LMA (in PBS) for 4 hours to overnight in a 37°C oven. The glass capillary array was retrieved and the redundant agarose liquid was scraped off with a cell scraper. The capillary was set on at room temperature bench for gelation for more than 5 minutes. Then I assembled approximately 10,000-15,000 oligo MMPs to one side of the agarose capillary array. While a strong magnet was present on the other side, I used a cell scraper to carefully spread the beads into a single layer, each bead being assembled into the capillary wells. For high filling rate, the beads had to be kept in a small input volume of around 0.5uL to 1uL, thus increasing concentration. Over-concentration led to multiple beads assembling into the capillary wells after scraping. The beads were then covered with 150uL of hot 5% agarose solution (conditioned with 1x TE or PBS) and immediately covered with a cover glass so that the agarose solution spread evenly into a thin film. This agarose cover ensures that the beads do not detach by agitating force or the capillary flow generated during the following cell assembly step. If the agarose concentration of the cover is not sufficient, the cover tended to tear off easily and was not able to perform bead retrieval needed after single cell RNA retrieval.

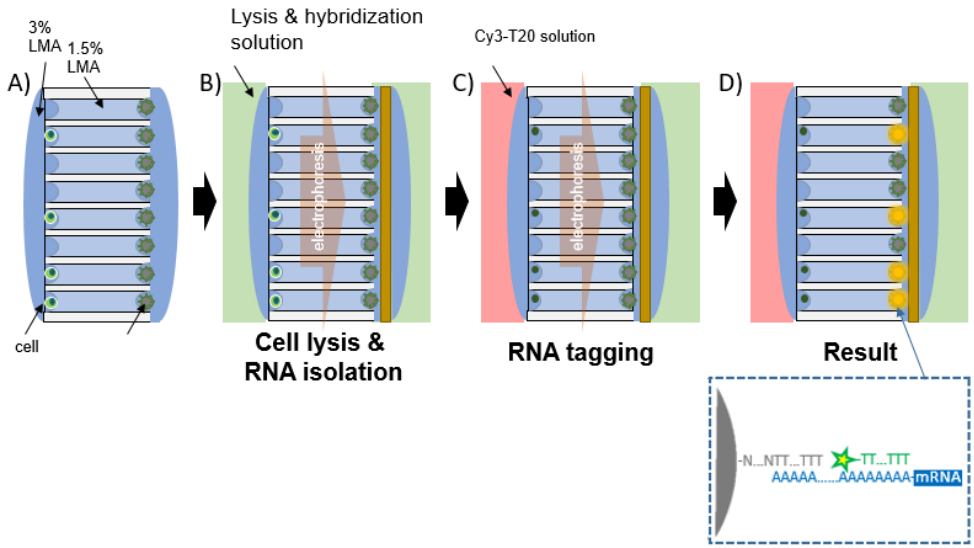

Figure 53. **Procedure of single cell mRNA capture and fluorescent tagging for imaging.** First a lysis & hybridization solution containing detergent (usually 0.1-0.5% SDS), high salt (usually 100-500mM LiCl) and buffer (10x TE) is filled in the MCA chamber. Then an electric field (usually 1V/cm) is immediately turned on to transfer mRNA along the capillaries. After 10-20 minutes the mRNA hybridize onto the oligo probes on the MMPs. Then Cy30-T20 is introduced into the MCA chamber for hybridization onto the poly A tails of the captured mRNA molecules. Therefore, the MMPs that contain the mRNA will be fluorescent.

If the immediate glass covering was not conducted, the 5% agarose liquid would not cover the entire array surface and solidify rapidly into a bulged droplet state. Although the 5% agarose liquid is highly viscous, the beads assembled into the capillary wells tended to remain assembled even after agarose coving probably due to the strong adhesion between the bead and the capillary agarose occurred by cell scraping. Next, the array was then placed on a double-sized glass slide (75 mm x 50mm) with a filter paper in between. Then, Kimtech tissue papers were placed on each side of the square array so that the edge of the tissue paper made a line contact with the edge of the array. The tissue papers were fixed with scotch tape to prevent slipping or bulging up. The thin filter paper was placed so that when capillary flow occurs within the capillary array, the water flow is made in contact with the tissue papers, leading to maximum capillary flow. Without the filter paper, the capillary flow tended to stop at the interface between the underlying glass slide and the capillary array. Next, Hoechst-stained cells were collected, counted and 1-2 x 10^5 cells worth of cell solution was mixed with PBS to make 200uL volume. The 200uL cell sample was then dispensed onto the opposite side of the capillary array where beads were assembled. In case if the capillary array was let at ambient condition for too long, thus leading to capillary array agarose drying, approximately 5-10uL of PBS was dispensed on the cell assembly plane and scraped with cell scraper before cell dispensing. This acted as a priming step for proper capillary flow to occur. After

cell dispensing, capillary flow occurred automatically and was let at ambient condition until all the cells were assembled into the capillary arrays and the cell solution was almost soaked completely by the tissue papers. Then 100uL of 1.5% LMA solution (in PBS) was dispensed onto the cell array plane and was let at ambient condition for gelation for about 5 minutes. Then the entire construct was imaged with a fluorescence microscope to check the cell assembly status. Next, the construct was inserted into the holder I previously explained. The running buffer was "275mM LiCl, 10x TE, 0.2% SDS, and 0.1x diluted RNase Later solution" for the inner chamber and 0.5x TBE for the outer chamber. As soon as the chamber was filled with running buffer, 1V/cm of electric field was given for 10-20 minutes. If available, the entire electrophoresis bath was submerged in an ice bath to prevent heating. Also, it was useful to performed initial strong 5V/cm field for 1 minute so that the lysed mRNA molecules entered the capillaries without loss by diffusion. After 10-20 minutes of electrophoresis, I added 1uL of 100uM Cy3-T30 probes into the running buffer and conducted electrophoresis for a further 10-20 minutes with 1V/cm electric field. The result was imaged with a fluorescence microscope. Under the microscope, when imaged from the cell array side, the beads assembled at the other side was recognizable as darker spots compared to bead non-assembled spots. The Hoechst stain tended to be almost removed after the electrophoresis step probably due to the SDS detergent. However, the nucleus (DNA) sill remained at the

original position and was recognizable.

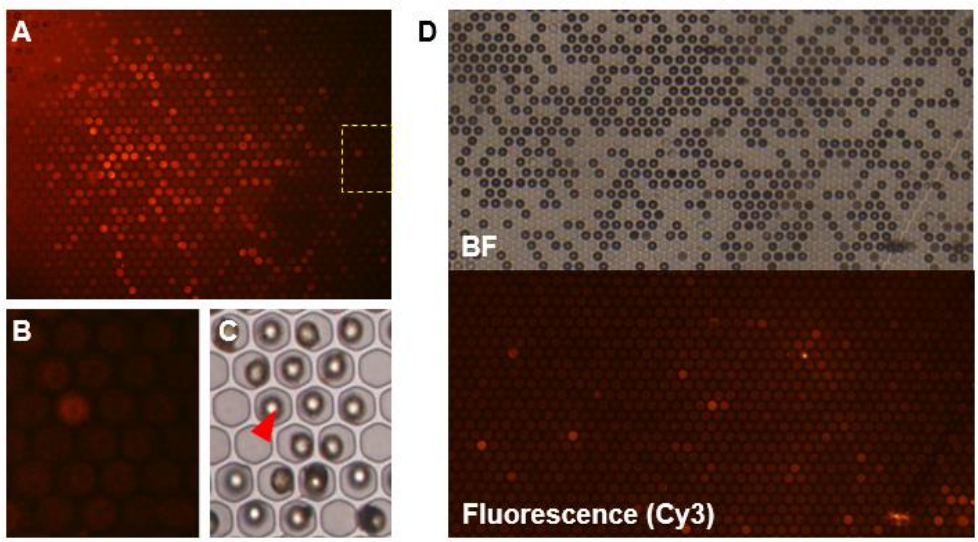

Figure 54. **Experiment result of mRNA capturing from single cells and fluorescent imaging.** From both experiments (A-C and D), the fluorescence signals show digital patterns rather than continuous pattern. This indicates proper mRNA capture without cross contamination with adjacent capillaries.

When imaged from the bead side, there were beads that showed brighter fluorescence compared to environment or other beads. These bright fluorescent beads were patterned in a digital fashion and not as a continuous gradient. Meaning, If there was a fluorescent bead among a group of beads in close contact, the neighboring beads didn't have any higher than environment fluorescence. This was a good indication that the mRNA molecules did not diffuse across neighboring capillaries. So, it seemed that this capillary array approach solved the cross contamination problem the original agarose array suffered from.

Next, I had to verify that the fluorescent beads were indeed capturing mRNAs from the cells corresponding to the same capillary and not from other neighboring capillaries. For this I had to match the cells' positions and the beads' positions and see if only capillaries with cell on one side and bead on one side produce fluorescent beads. If either the cell was missing or the bead was missing, there should not be any fluorescent beads. For this, I conducted the above experiment but with lower density of cells and beads to make capillaries with paired cell and bead be rare. The result showed that indeed, only capillaries having pairs of cell and bead show bright fluorescence.

Next, I wanted to measure, although qualitative, the number of mRNA molecules retrieved by these beads. For this I had to make a standard curve and measure the number of probes attached to each bead. For the standard curve, I

imaged a fluorescent solution with serial dilution containing Cy3 as the fluorescent T30 probe. The fluorescence intensity was quantified by Image J to make a standard curve. Next, for the probe concentration, I used Qubit ssDNA kit. I used a fixed amount of beads for ssDNA measurements. The result showed that each oligo MMP had around 1.47 x 10^8 probes attached on its surface. Then I mixed the oligo MMPs with Cy3 A30 in 1x TE buffer and performed vortex until the beads were saturated with the probes. The beads were then washed and imaged with a fluorescence microscope to quantify its fluorescence intensity using Image J. Also, images taken from the single cell electrophoresis experiment result was also analyzed with Image J. By positioning the fluorescence intensities of the saturated beads (which acts like a positive control) and the single cell electrophoresis beads along the standard curve, I was able to roughly measure the number of mRNA molecules retrieved by the beads. Also, since the poly A tails of mammalian cells are around 50-100nt, which means that multiple Cy3-T30 probes could attach to one mRNA molecule, I compensated the resulting calculation. The result showed that the beads recovered approximately 10^6 mRNA molecules on average. This is in good agreement with the number of mRNA molecules inside a single mammalian cell.

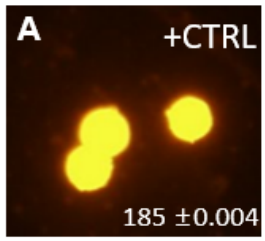

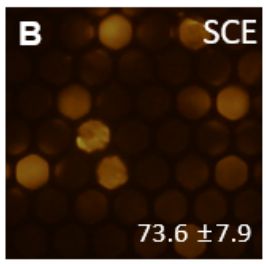

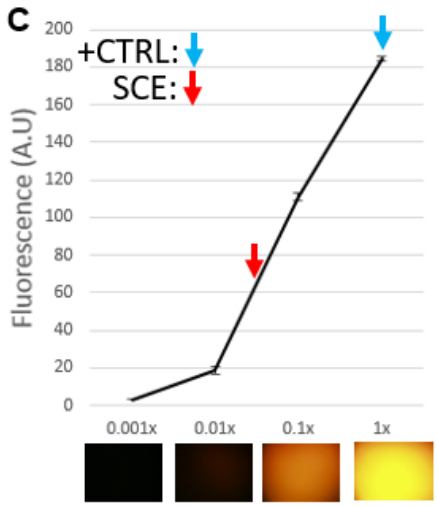

D

	Probe conc. (Qubit)	Cy3 intensity (A.U.)	Cy3T20 probes captured per bead	mRNA captured per bead
+CTRL	1.47 x 10^8 probes/bead	1x	Max	-
SCE		~0.05x	~5 x 10^6	~10^6

* polyA tail length: 50-100nt
* Probe length : 20nt
* No. mRNA per cell : 10^5 - 10^6

Figure 55. **Fluorescence intensity and standard curve based mRNA capture rate deduction of Single cell electrophoresis (SCE) experiment result.** First the mRNA capturing probe concentration on these MMPs were measured with Qubit ssDNA kit. Then the fluorescence intensity of the MMPs of a positive control (saturating cy3T20 probe hybridization) and SCE result MMPs were measured with a fluorescence microscope and quantified with Image J. Then a standard curve was created using a serial dilution of Cy3 solution. The positive control (+CTRL) and SCE fluorescence was positioned at the standard curve to deduce the Cy3 probe concentration on the SCE MMPs. Then the number of Cy3 T20 probes hybridized onto a single mRNA molecule was used to finally deduce the number of mRNA

molecules hybridized onto the MMPs.

7.2.2 Bead harvest and RT-PCR

To retireve the beads from the capillary array, I tried many approaches. First I tried solution dispensing and pipette vortexing, but the force was not enough to remove any beads from the array. Adding high concentrations of detergents like Tween 20, Triton X, SDS had no effect. I also tried using freeze-thaw cycling, and submerging in anionic buffers. I also tried sonication. For this. MMP-assembled chips were submerged in room temperature 6X SSC solution. The tube was then submerged in a sonicating water bath and was sonicated for 2-12 minutes. Samples were imaged every 2 minutes of sonication. After 5 consecutive 2min incubation in 6x SSC, For this experiment. initially approximately 1000 beads were assembled to the chip. After 12minutes of sonication, there were 200 beads left. this was a significant improvement in bead retrieval. Compared to Adaptive Focused Acoustics™ (AFA) Technology used for DNA random shearing, this water bath based method had smaller engery transfer. Although there was an anticipation that dsDNA or RNA:cDNA might be sheared by sonication, previous reports showed thatwater bath sonication doesn't hamper DNA hybridization (Environ Health Toxicol. 2014; 29: e2014007.). Also, experiments with dsDNA showed that sonication does not hamper with hybridization. However, the problem was that sonication induced shattering of the capillary array itself and the retrieval yield was

not sustainably high over repeat experiments

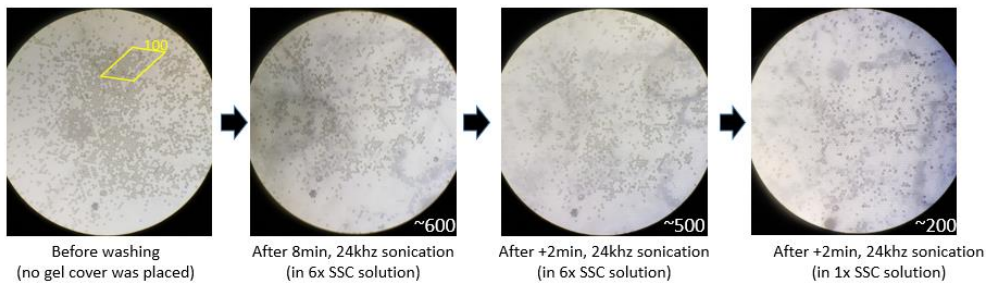

Figure 56. **Result of MMP retrieval method using sonication.**

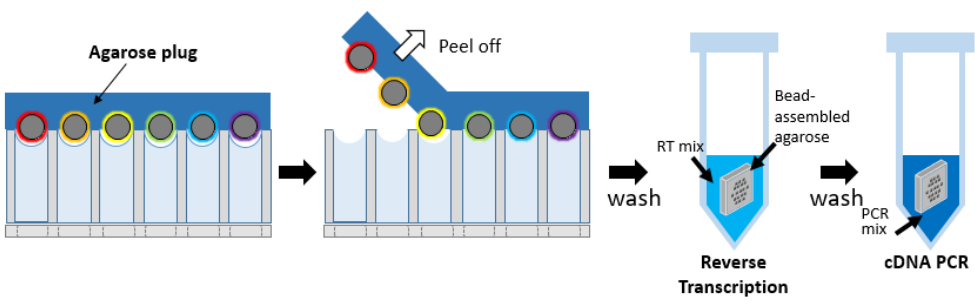

Figure 57. **Method of retrieving the MMPs using a high concentration agarose film and peel-off.** The resulting films can be directly used for reverse transcription and PCR since agarose does not prevent these reactions.

Finally I came up with a simple solution of using high concentration

agarose covering. As explained before, the beads can be covered with high, 5% agarose film. And by simply peeling off this film the beads tended to peel off with the film. This is because the film has higher adhesion force to the bead than the underlying capillary agarose because of its higher agarose concentration. The retrieved agarose film was cut into smaller pieces and added into a reverse transcription reaction mix (30uL total volume with the same composition explained above except to account for the additional volume of the agarose film). Agarose film itself didn't seem to hamper the reverse transcription and following PCR reaction. So I simply performed the following RT-PCR at the presence of agarose film. This conveniently removed the need for actually retrieving the beads from the agarose film.

7.2.3 Validation using Sanger sequencing

To validate that I indeed obtained proper cDNAs, I decided to perform Sanger sequencing. For this, I firsted performed TOPO cloning of the amplified cDNAs. A minimum of 20ng of cDNA was mixed with TOPO cloning buffer and Topo isomerase and incubated at room temperature overnight. The mixture was then dispensed into a 100uL competent cell sample and incubated on ice for more than 30 minutes. The cell sample was then incubated in a 42°C for 30-40 seconds and on ice for 2.5 minutes. Then 900uL of SOC buffer was introduced and the sample was

incubated in a 37°C incubator with 500 rpm for 30-40 minutes. 300-500 uL of the sample was then dispensed on an LB agar plate containing 100ug/mL ampicillin and 50ug/mL kanamycin. After overnight incubation in a 37°C incubator, the clones were picked and dipped into 10uL Taq polymerase PCR mix containing 0.1uM of M13F and M13RpUC. PCR was performed as given in the TOPO kit user guide. The Taq polymerase samples that contained positive cDNA bands under gel electrophoresis was purified with KAPA purification kit and was sent to Macrogen for standard Sanger sequencing.

The sequencing results showed the cDNA structure as expected. It should be noted that the beads used for this cDNA amplification and verification experiment did not contain any cell barcode. The sequencing result showed the primer and UMI, poly T(A) sequence, and cDNA sequence of expected species.

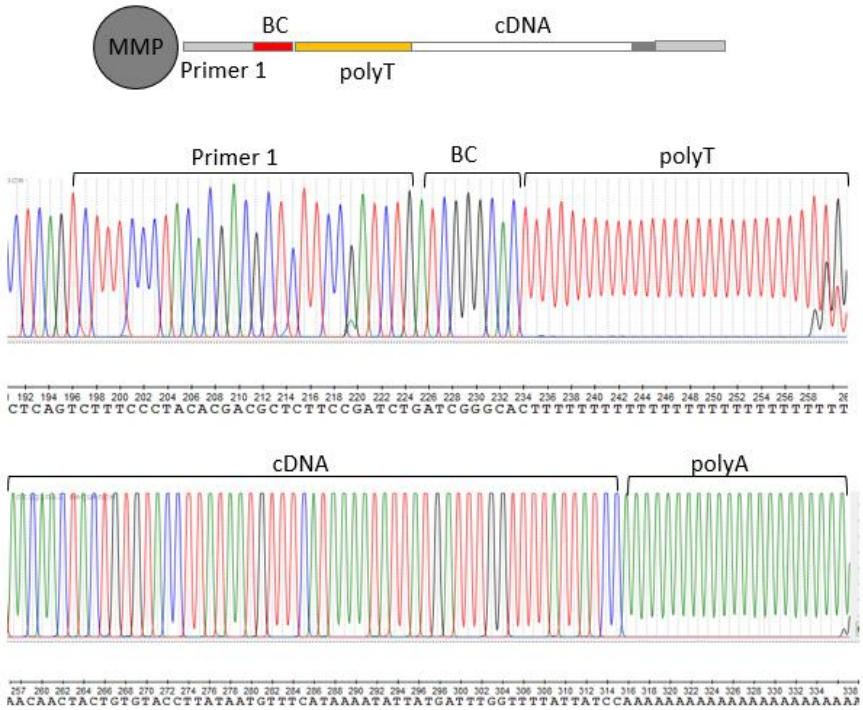

Figure 58. Sanger sequencing result of captured mRNA.

7.2.4 Discussion

The technique shown in this chapter can be further modified for commercialization. As an intellectual practice, I designed a model kit to show in theory, how users might use this technique.

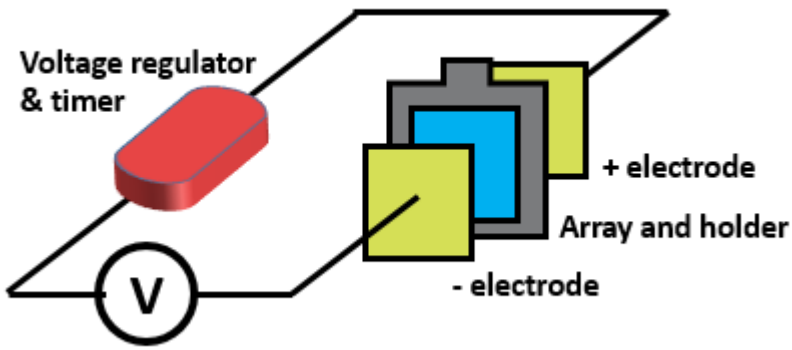

Figure 59. **Circuitry of the electrophoresis device.**

The circuitry of the device would be the same as any electrophoresis device. But unlike conventional electrophoresis devices which uses wire type electrodes, the electrodes for this device would have to be plate-like such that the electrophoretic field would be perpendicular to the capillary array surface.

The detailed steps of using my model kit would be as follows. First, the distributor of the kit would provide users with a custom electrophoresis device and a consumable kit. When actually performing the experiment, users would then dispense their cell sample of interest onto the array chip pre-assembled with RNA

capturing microparticles on the opposite side of cell dispensing surface. After sufficient drying out of the cell sample medium, user would dispense liquid hydrogel (or possibly other liquid covering material) onto the cell array and let solidify. Users would then assemble this cell/microparticle array chip into the electrophoresis device and fill the chamber with designated buffer. The electric field of the device is then immediately turned on for electrophoretic retrieval of RNA onto the microparticles within several minutes. Users would then remove the chip from the device and either retrieve the beads for RT-PCR or submerge the entire chip in a storage buffer (containing RNase inhibitor). Then either the barcoded cDNA or the entire chip containing mRNA-captured particles could be sent to an NGS servicing department (or company) for further NGS library preparation and sequencing.

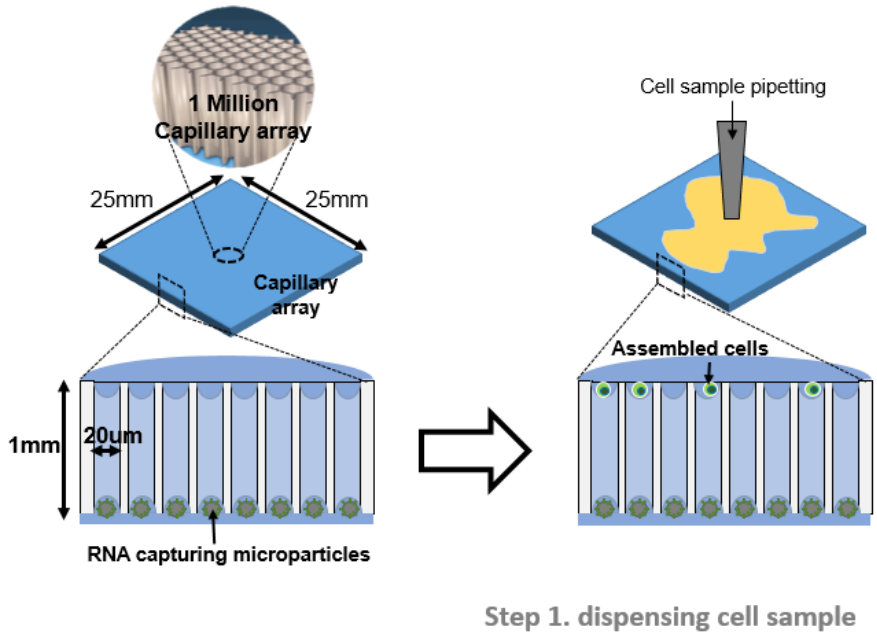

Figure 60. **The model kit protocol part 1.** The bead assembled MCA can be prepared by the kit manufacturer and distributed to users. Cells are assembled by simple dispensing by the user.

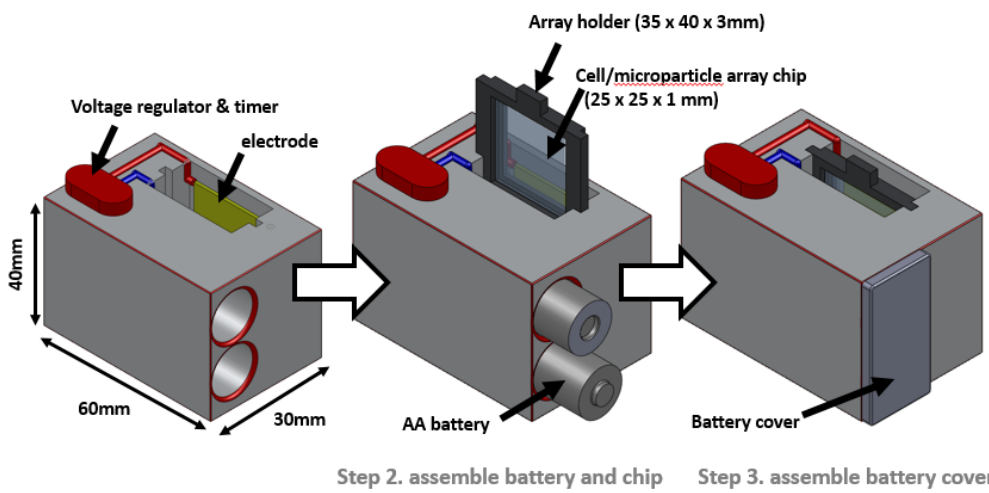

Figure 61. **The model kit protocol part 2.** The MCA is inserted into the electrophoresis device and the batteries are assembled as well.

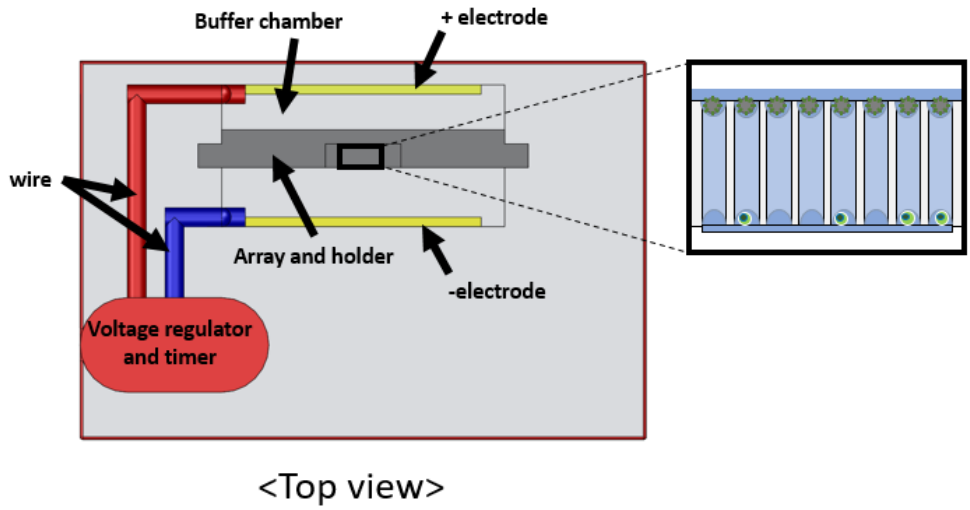

Figure 62. **The top view after the MCA and batteries are assembled.** The voltage regulator and timer is connected to the electrodes which are placed on both side of the MCA cell, bead array surfaces.

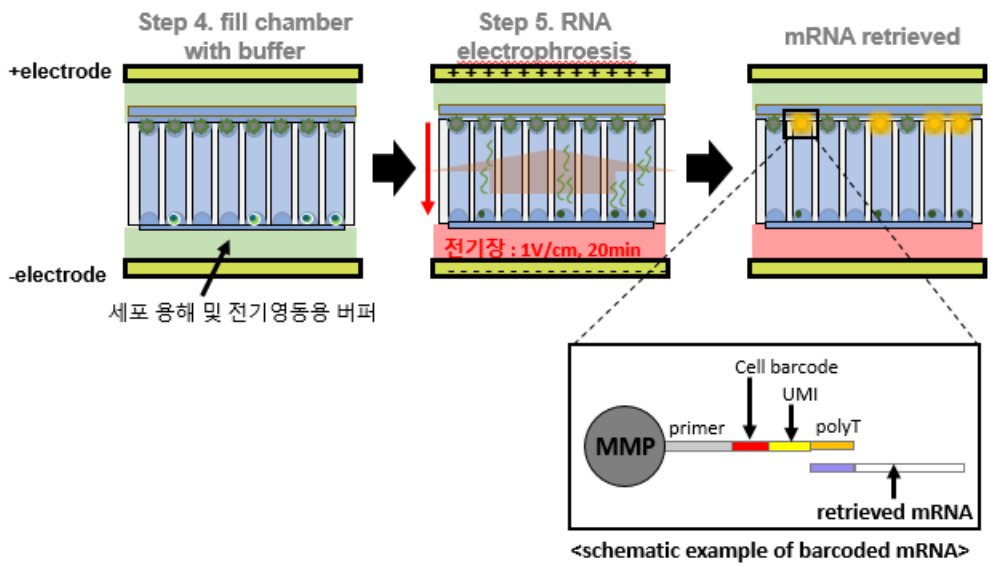

Figure 63. **The model kit protocol part 3.** The chamber is filled with buffer and

electrophoresis is performed to capture the cell mRNA onto the RNA capturing beads.

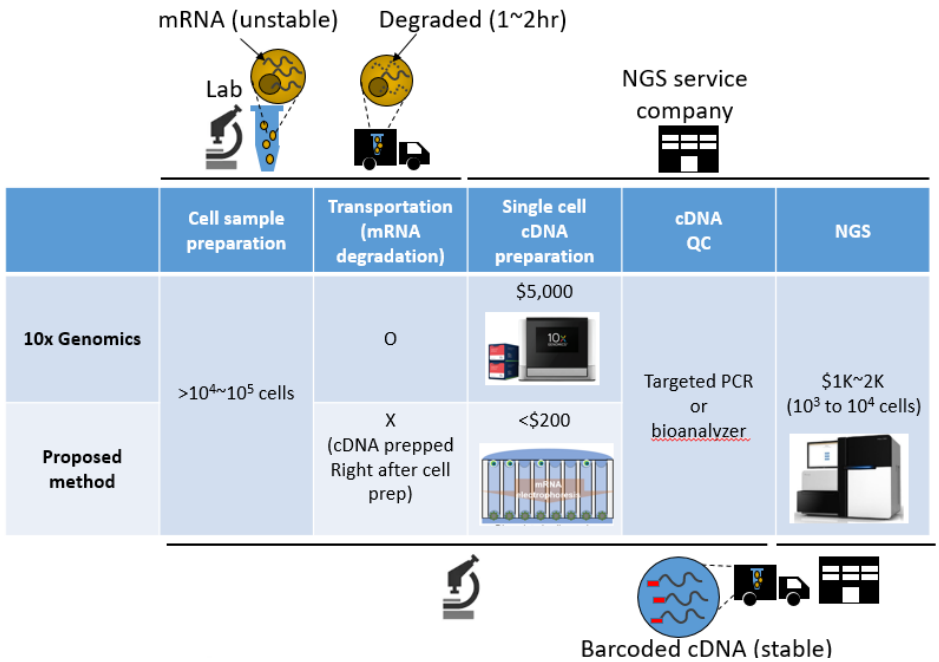

Figure 64. **Comparison of the commercialized kit and proposed method.** Unlike the commercialized kit, proposed method doesn't require any live cell delivery and RNA capture QC can be done with lower price.

Chapter 8 : Summary

In this chapter, I summarized the novel works of this thesis paper.

I created a novel noncovalent hydrogel to solid bonding method. This required a solid type hydrogel glue which utilized the diffusive monomer to act as an intertwining polymer network at the presence of UV irradiation. It also utilized the chemical anchorage of the intertwining network to the hydrogel glue for further bonding strength increase. The hydrogel glue could act as a two-sided tape between noncovalent hydrogel and solid surfaces pretreated with acryl functional group activation. With this bonding method, I created novel functionalities such as microchannel patterned hydrogel intestine model, anti-disconnect construct, and self-aligned self-healing system. I was also able to generate a microcapillary agarose hydrogel array for single cell RNA retrieval.

The virtues of this bonding method are as follows. First, the application of this bonding method was verified for macroscale as well as microscale. Therefore it could be applied in numerous fields in multiscale systems. This method will offer new applications for various fields including in vitro assays, soft robotics, and tissue engineering. Also, this method could be applied to various noncovalent hydrogels and solids since the bonding method is designed to be applicable to such materials

without much dependency of the hydrogel/solid materials' matrix backbone.

The shortcomings of this method includes the factors as follows. First, it requires UV crosslinking thus limiting application to live cell/tissue applications. One can overcome this with visible light-activated initiators such as eosin Y albeit with less efficiency. Next, the method requires monomer initiator diffusion, therefore the application would be less efficient for matrixes that have low diffusion rate.

The single cell RNA retrieval application shown in chapter 6 and 7 can be further expanded to single cell DNA and RNA parallel retrieval as shown in chapter 6. This is because agarose matrix has the ideal pore size to selectively let RNA diffuse (or retrieved by electric field) while genomic DNA being fixed to the original position. So one could first extract RNA by cell lysis and electrophoresis, perform subsequent genomic DNA shearing or enzymatic amplification (such as MDA) and then perform a second electrophoresis for genomic DNA retrieval. The genomic DNA and RNA can be tagged separately by designing the probes with different sequence. For example, a polyT probe can be used for capturing mRNA while an anti-Tn5 transpose adapter being used to capture Tn5-transposase-sheared genomic DNA. This way one could tag both mRNA and genomic DNA (or open chromatin) from the same single cell, simultaneously from multiple single cells. This topic will be dealt in my future studies.

Bibliography

[1] J. Y. Sun. X. Zhao, W. R. K. Illeperuma, O. Chaudhuri, K H. Oh, D J. Mooney, J. J. Vlassak and Z. Suo, *Nature*, 2012, 489,133–136.

[2] H. Yuk, T. Zhang, S. Lin, G. A. Parada and X. Zhao, *Nat. Mater.*, 2016, 15, 190–196.

[3] H. Yuk, T. Zhang, G. A. Parada and X. Zhao, *Nature Commun.*, 2016, 7, 12028.

[4] S. Hong, D. Sycks, H. F. Chan, S. Lin, G. P. Lopez, F. Guilak, K. W. Leong and X. Zhao, *Adv. Mater.*, Vol.27, 27, 2015, 4035–4040.

[5] Yu Shrike Zhang and Ali Khademhosseini, *Science*, 2017, 356, 6337.

[6] H. Yuk, S. Lin, C. Ma, M. Takaffoli, N. X. Fang and X. Zhao, *Nat. Commun.*, 2017, 8, 14230.

[7] P. Calvert, *Adv. Mater.*, 21, 2009, 743–756.

[8] J. Zhu and R. E. Marchant, *Expert. Rev. Med Devices*, 2011, 8(5), 607–626.

[9] T. Billie, M. Vandenhaute, J. Schelfhout, S. V. Vlierberghe and P. Dubruel, *Biomaterials*, 2012, 33, 26,6020–6041.

[10] S. Fernandez-Cossio, A. Leon-Mateos, F. G. Sampedro, and M. T. C. Oreja, *Plast. Reconstr. Surg.*/ 2007, 120(5):1161-9.

[11] D. L. Taylor and M. in het Panhuis, *Adv. Mater.*, 28, 2016, 9060–9093.

[12] Y. Ling, J. Rubin, Y. Deng, C. Huang, U. Demirci, J. M. Karpae and A.

Khademhosseini, *Lab Chip*, 2007, 7, 756–762.

[13] K. Chung, et al., *Lab Chip*, 2011, 11, 3689-3697

[14] Y. Li, X. Yan, X. Feng, J. Wang, W. Du, Y. Wang, P. Chen, L. Xiong, and B. F. Liu, *Anal. Chem.*, 2014, 86, 10653−10659.

[15] N. N. Kachouie et al., *Organogenesis*, 2010, 6(4): 234-244.

[16] I. Wong, S. Atsumi, W. C. Huang, T. Y. Wu, T. Hanai, M.-L. Lam, P. Tang, J. Yang, J. C. Liaoc and C. M. Ho, *Lab Chip*, 2010, 10, 2710–2719.

[17] P. Nghe, S. Boulineau, S. Gude, P. Recouvreux, J. S. V. Zon and S. J. Tans, *PLoS ONE*, 2013, 8, 9, e75537.

[18] S. Y. Cheng, S. Heilman, M. Wasserman, S. Archer, M. L. Shulerac and M. Wuab, *Lab Chip*, 2007, 7, 763–769.

[19] K. Nagamine, K. Okamoto, H. Kaji and M. Nishizawa, *J. of Biosci. and Bioeng.*, 118, 2014, 1, 94–97.

[20] D. Wirthl et al., *Sci. Adv.,* 2017, 3, no. 6, e1700053.

[21] J. Saito et al., *Polym. Chem.*, 2011, 2, 575–580.

[22] Q. Liu, G. Nian, C. Yang, S. Qu and Z. Suo, *Nat. Commun.*, 2018, 9, 846.

[23] D. W. Fong, and D. J. Kowalski, Joumal of Polymer Science: Part A: Polymer Chemistry, 1993, 31,1625-1627.

[24] F. Ding, et al., Soft Matter, 2015, 11, 3971-3976.

[25] O. A. C. Monterio Jr. et al., *International Journal of Biological*

Macromolecules, 1999, Vol. 26, Issues 2-3, 119-128.

[26] A. Serrero et al., *Biomacromolecules*, 2010, *11* (6), pp 1534–1543

[27] Q. Chen , L. Zhu , C. Zhao , Q. Wang and J. Zheng, *Adv. Mater.*, 2013, 25, 30, 4171–4176.

[28] X. Li, Q. Yang, Y. Zhao, S. Longa and J. Zheng, *Soft Matter*, 2017, 13, 911.

[29] J. Wei, J. Wang, S. Su, S. Wang and J. Qiu, *J. Mater. Chem. B*, 2015, 3, 5284--5290.

[30] Q. Chen, D. Wei, H. Chen, L. Zhu, C. Jiao, G. Liu, L. Huang, J. Yang, L. Wang, and J. Zheng, *Macromolecules*, 2015, 48 (21), 8003–8010.

[31] R. Rivlin, A. G. Thomas, *J. Polym. Sci. Part A: Polym. Chem.,* 1953, 10, 291

[32] G. Gao, G. Du, Y. Sun and J. Fu, *Appl. Mater. Interfaces*, 2015, *7* (8), 5029–5037.

[33] Y. Okumura and K. Ito, *Adv. Mater.*, 2001, 13, 7, 485–487.

[34] K. Haraguchi and T. Takehisa, *Adv. Mater.*, 2002, 14, 16, 1120-1124.

[35] V. I. Egorova, I. V. Schastlivtsevb , E. V. Prutc, A. O. Baranovc, and R. A. Turusovc, J. of Biomechanics, 2002, 35, 1417–1425.

[36] Y. Liao et al., *Ind. Eng. Chem. Res.*, 2014, *53* (27), pp 11193–11203.

[37] R. Abdelkader, and B. Mohammed, Bulletin of Chemical Reaction Engineering & Catalysis, 201611 (2), 170-175.

Abstract(국문초록)

배상욱 2014-31113

아가로스를 비롯한 noncovalent 하이드로겔들은 biocompatibility가 좋은 반면에 다른 고체 표면과의 접착력이 약해 그 활용성이 낮은 편이었다. 기존의 noncovalent 하이드로겔 접착 방법은 주로 기계적 고정방법에 많이 의존했는데 이는 일시적인 접착일 뿐이고, 동적 부품이나 복잡한 표면에는 적용이 어려웠다. 본 논문에선 접착면 toughness 증강을 도모하는, 그리고 활용성, 범용성이 좋은 하이드로겔 접착방법을 제시한다. 본 접착방법은 gelatin, alginate, agar, 그리고 chitosan등의 noncovalent hydrogel에 대해 적용 가능하다는 것을 보여줬다. 본 방법은 기계적 고정이 전혀 필요 없고, 액상 접착제나 하이드로겔 polymer backbone 수정을 요구하지 않는다. 또한 접착표면상에 미세구조들을 유지할 수 있다. 이 접착방법을 사용해서 전기미세유체, 단일세포전사체분석 등의 활용 예시들을 보여줬다. 본 접착방법은 이 외에도 *in vitro* 어세이, 소프트 로보틱스, 생체모방 등의 분야에 활용 가능할 것으로 예상한다.